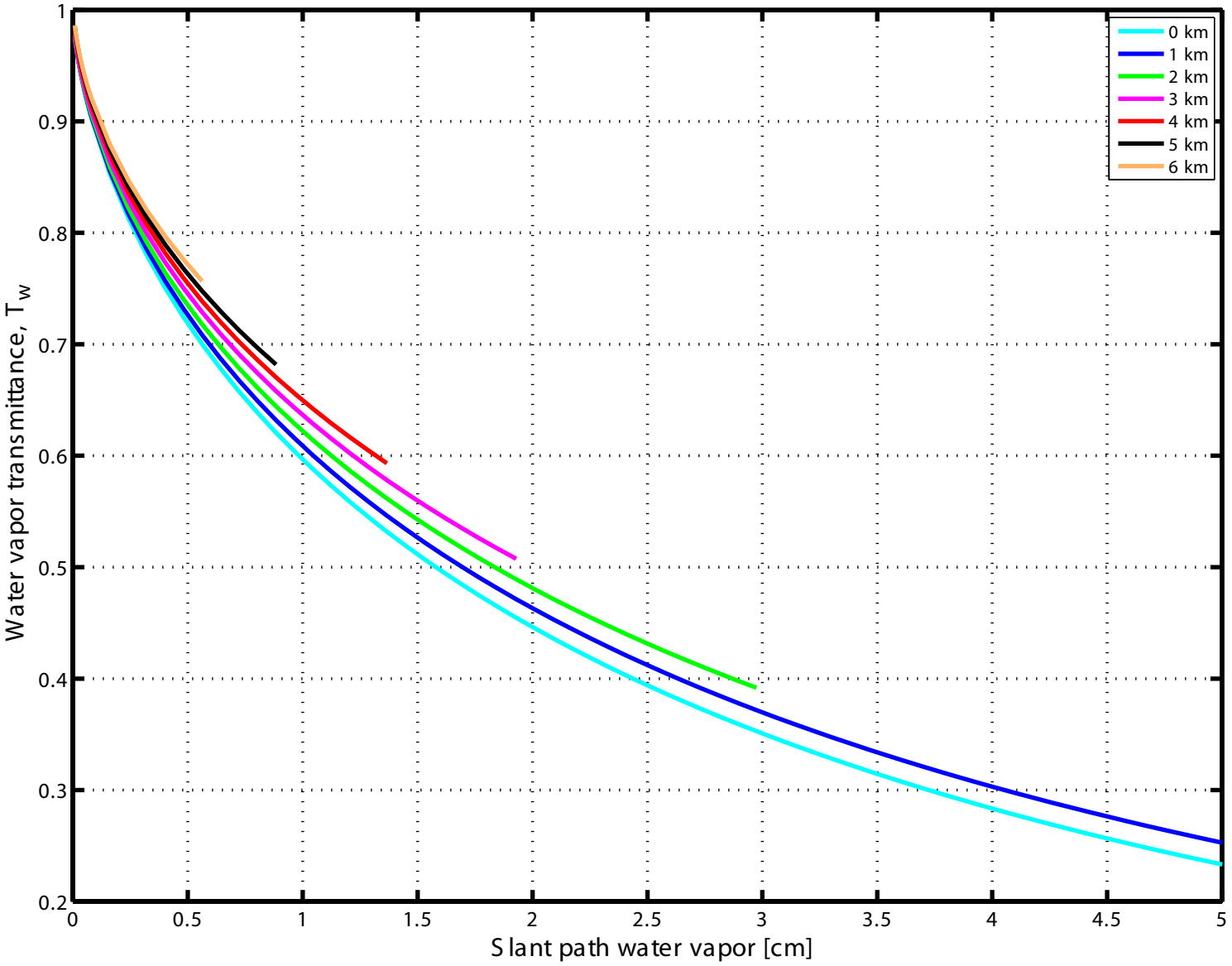

Figure 1. LBLRTM calculations of water vapor transmittance T_W as a function of slant path water vapor and aircraft altitude for the AATS-14 941-nm channel.

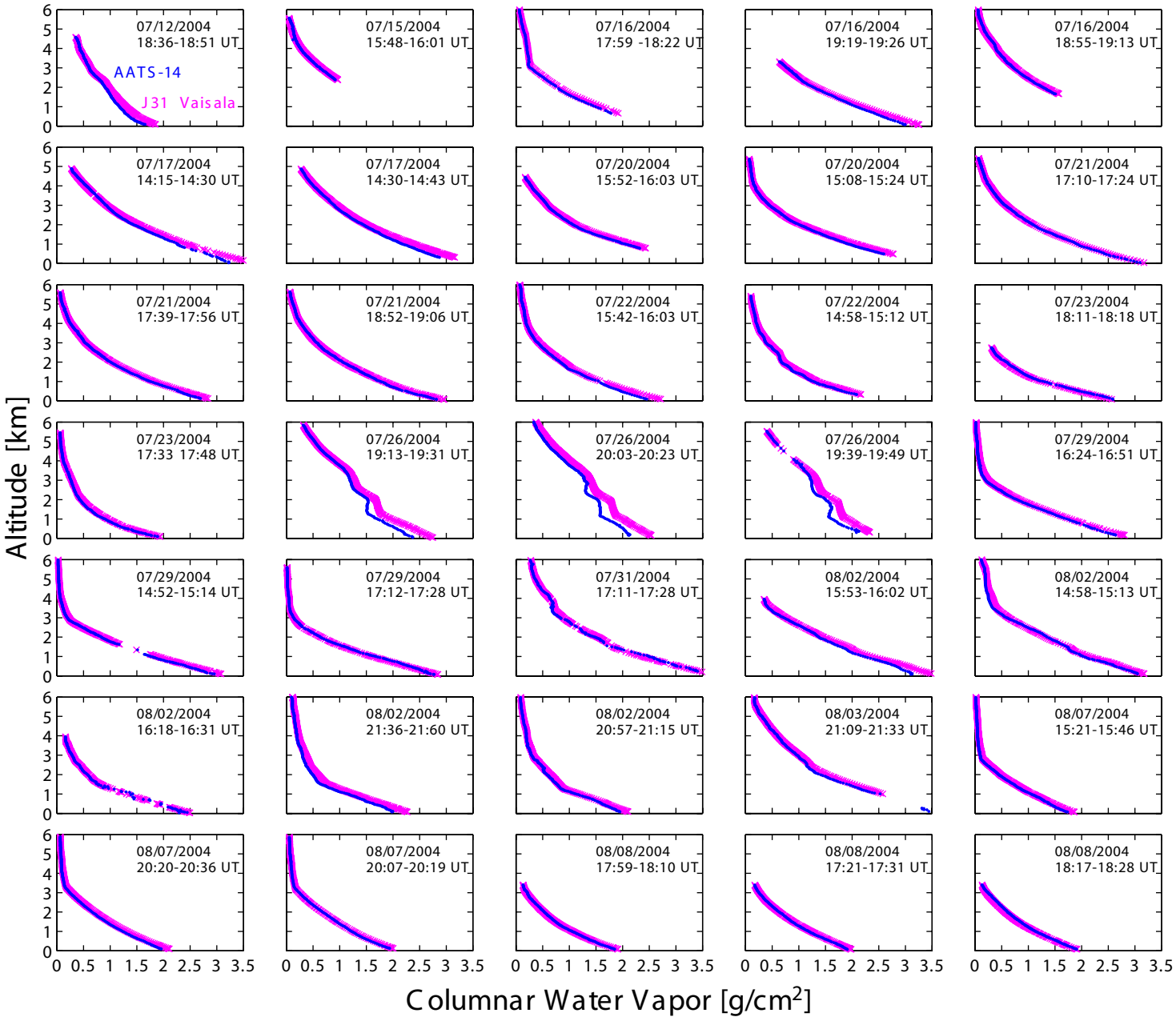

Figure 2. Vertical profiles of CWV calculated from measurements by AATS-14 and the J31 Vaisala HMP243 during INTEX-A/ITCT 2004. Vaisala values have been set equal to the AATS CWV at the top of each profile.

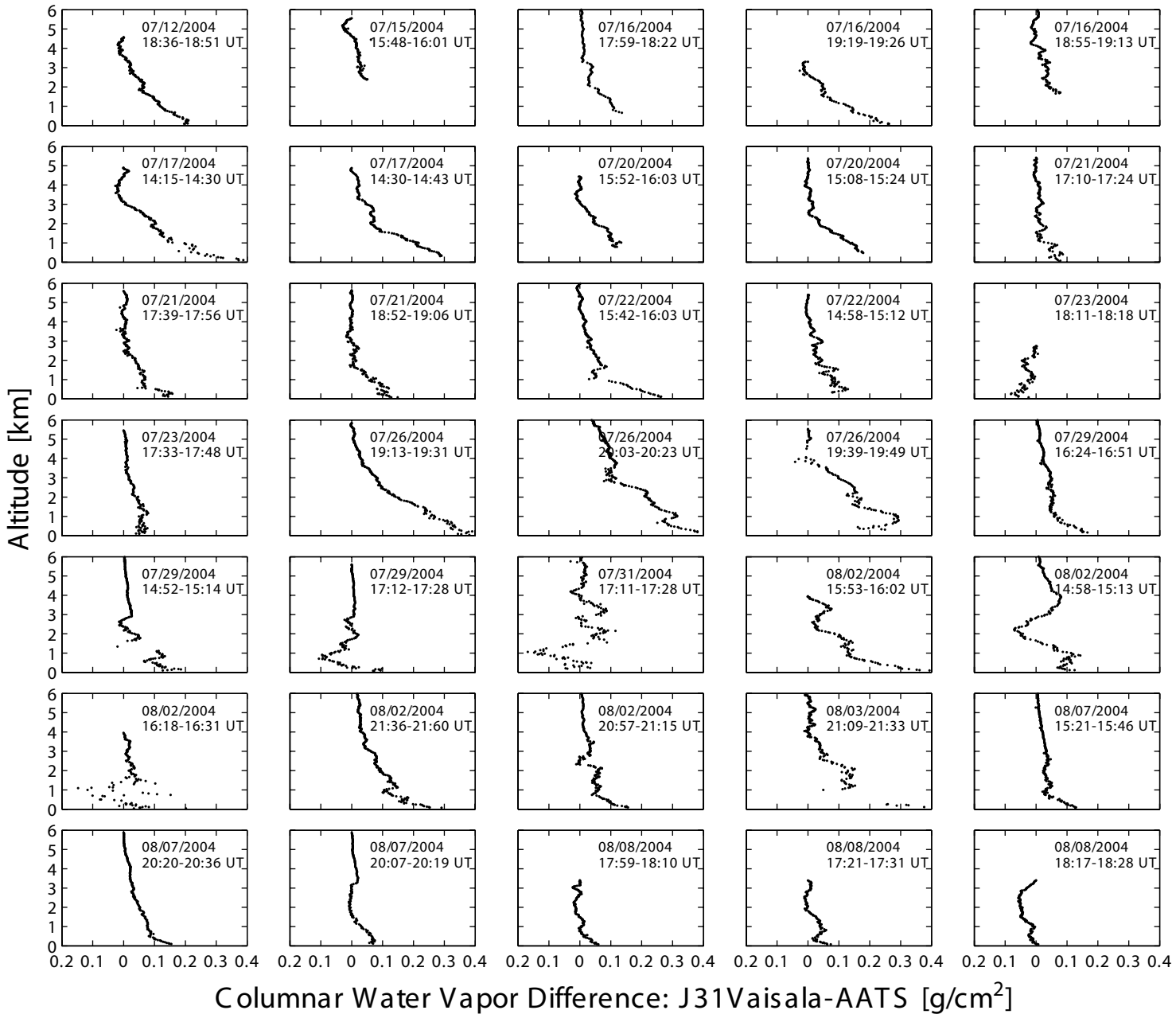

Figure 3. J31 Vaisala minus AATS-14 CWV differences for the vertical profiles shown in Figure 2.

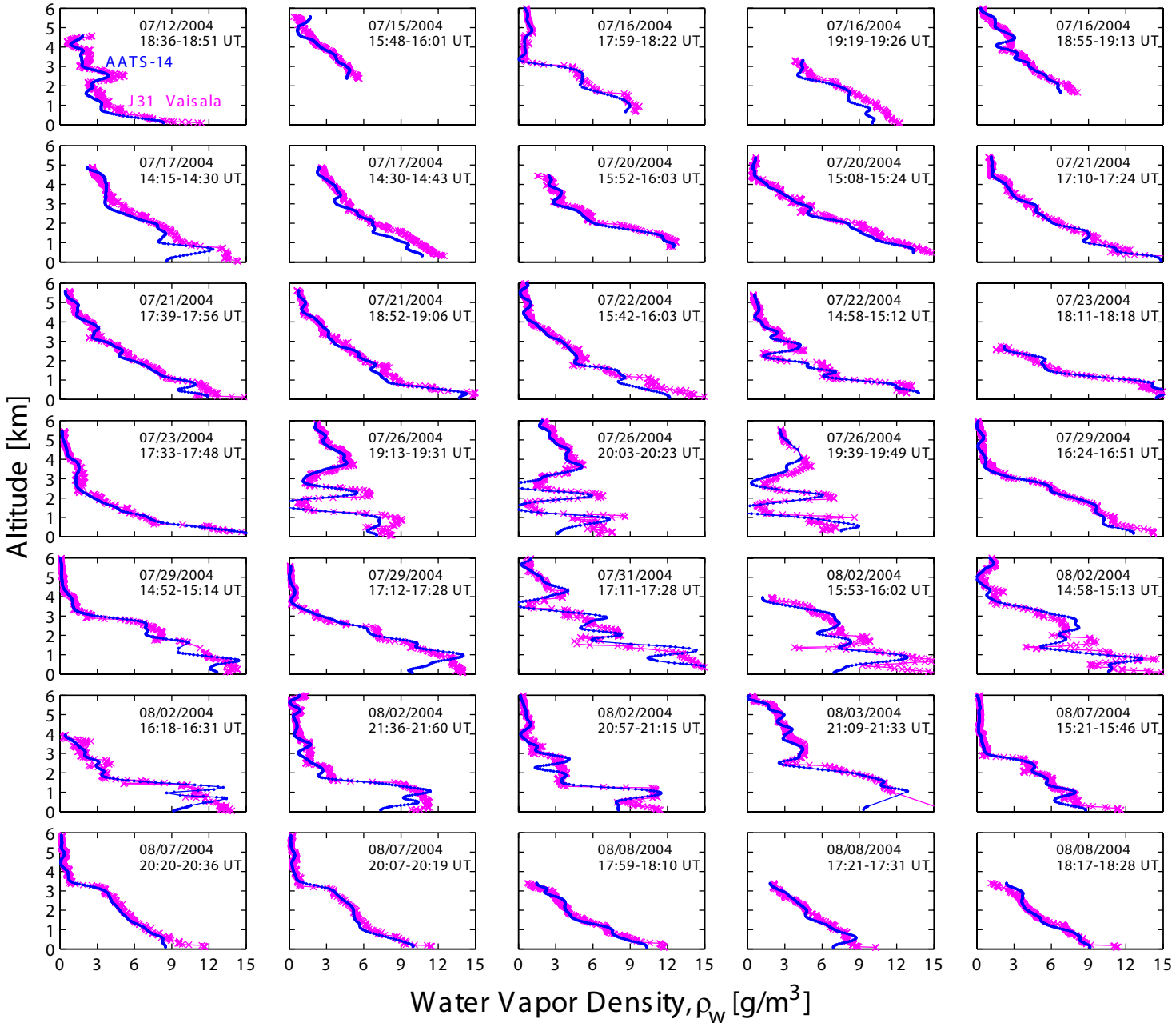

Figure 4. Vertical profiles of water vapor density, ρ_w, for the profiles shown in Figure 2.

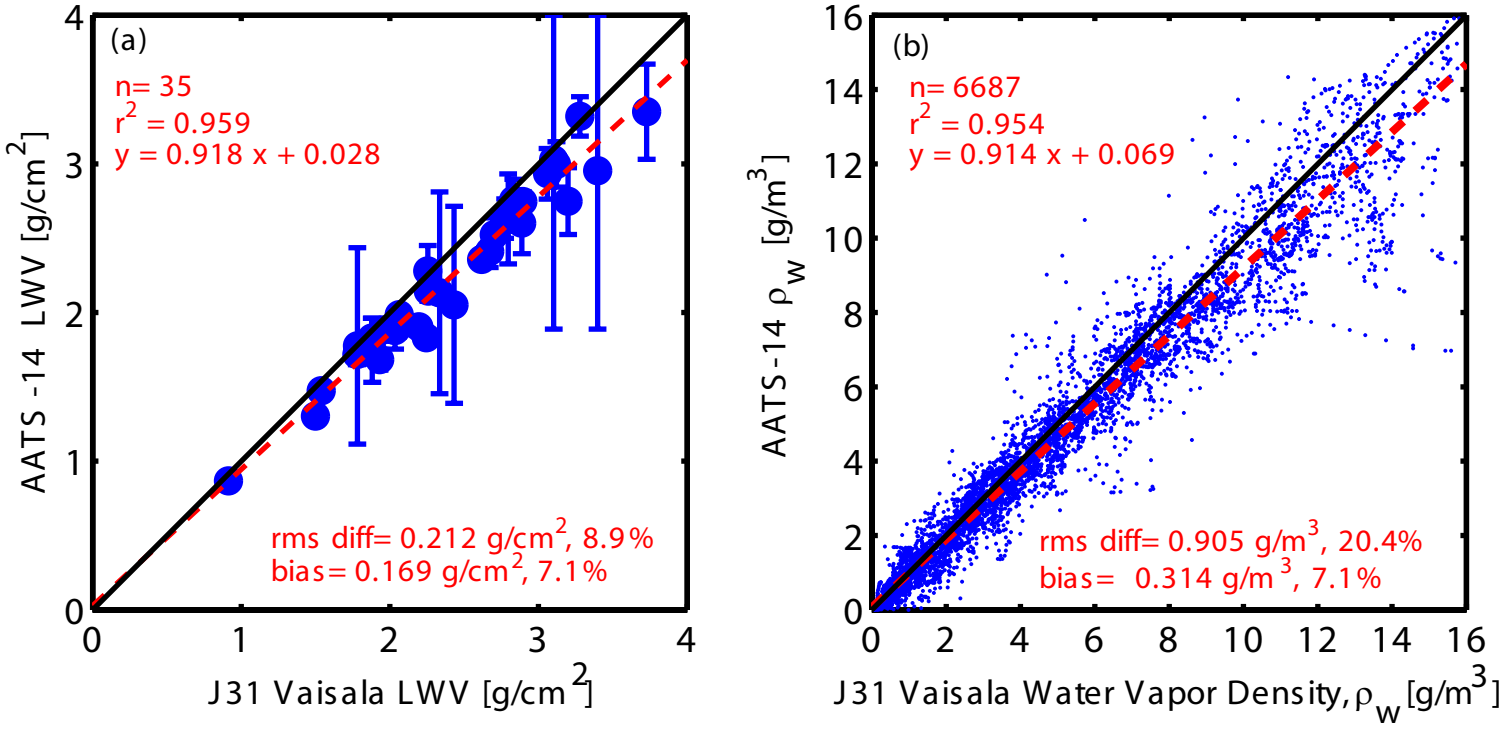

Figure 5. For the profiles shown in Figs. 2-4, scatterplots of AATS-14 and J31 Vaisala (a) LWV and (b) ρ_W for all profile altitudes.

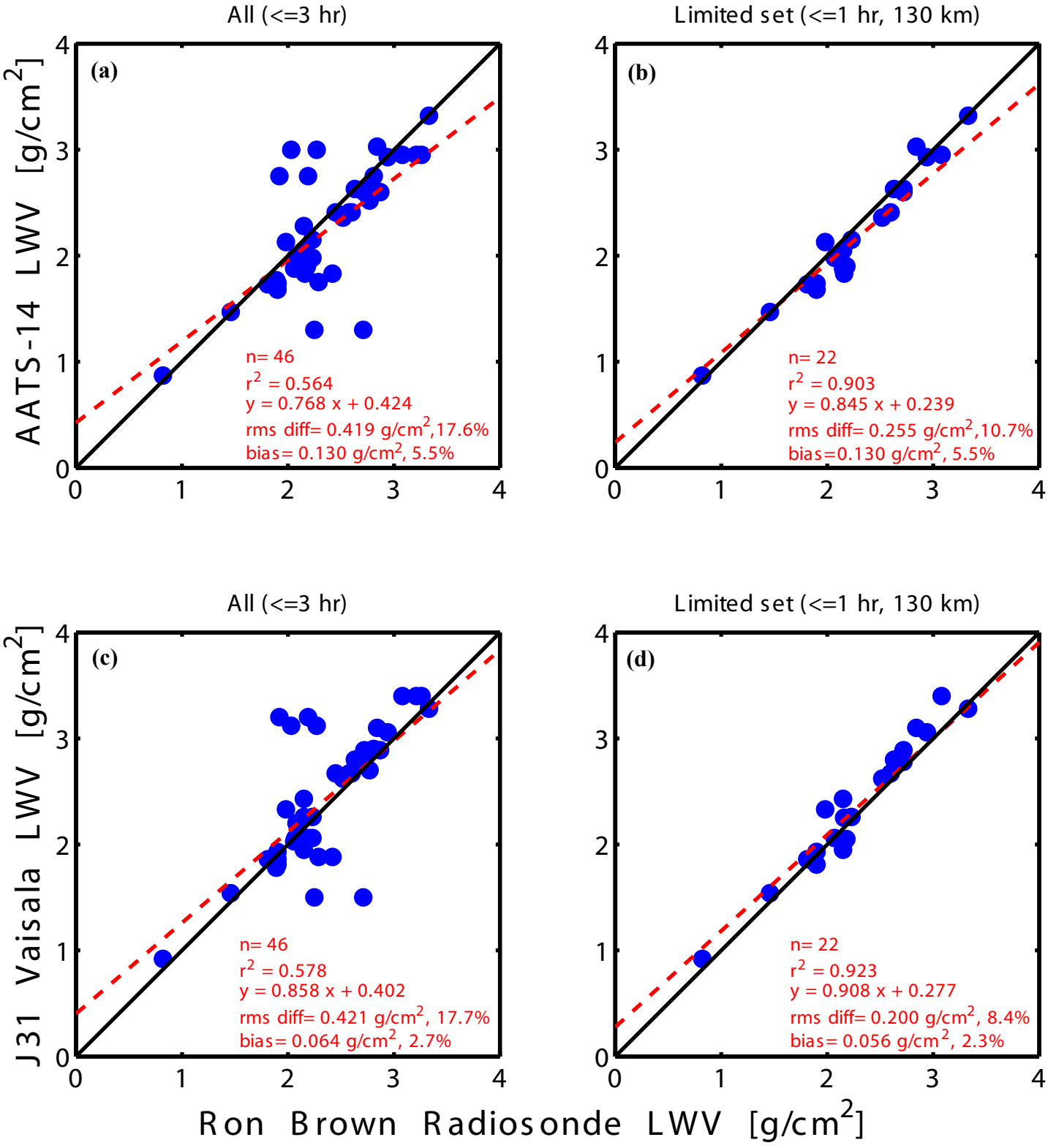

Figure 6. Comparison of LWV measured by AATS-14 and J31 Vaisala with Ron Brown radiosonde LWV for (a,c) all soundings within 3 hr of a J31 profile, and (b,d) only soundings within 1 hr and 130 km of a J31 profile.

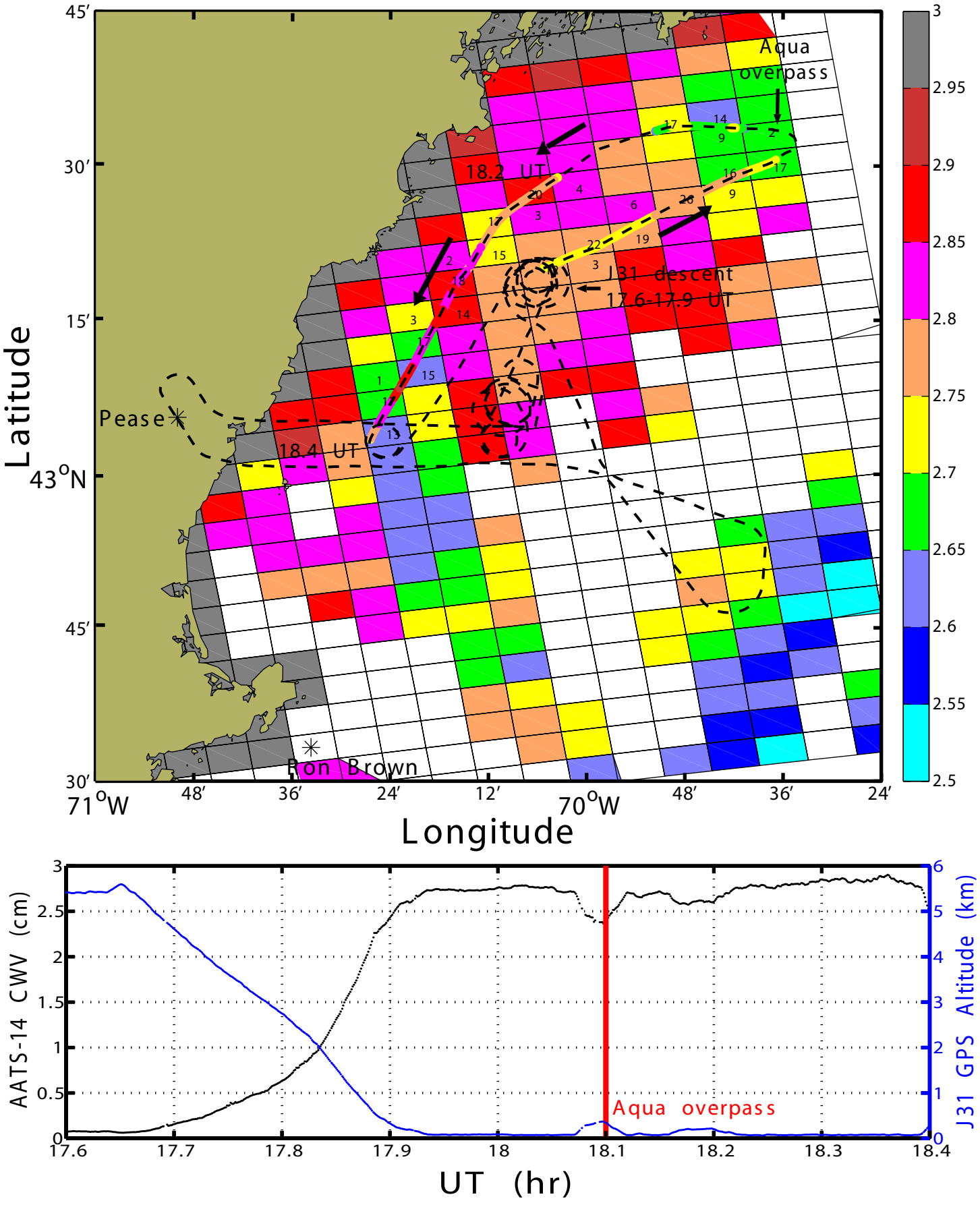

Figure 7. Top: map showing J31 flight track (black thin dashed line) overlaid on MODIS grid cells of color-coded MODIS IR TPW for Aqua overpass at 18.1 UT on 21 July 2004. The J31 flight track for the low altitude transect during the period 17.9-18.4 UT has been color-coded by AATS-14 CWV. Bottom: AATS-14 CWV and J31 altitude for the time period 17.6-18.4 UT.

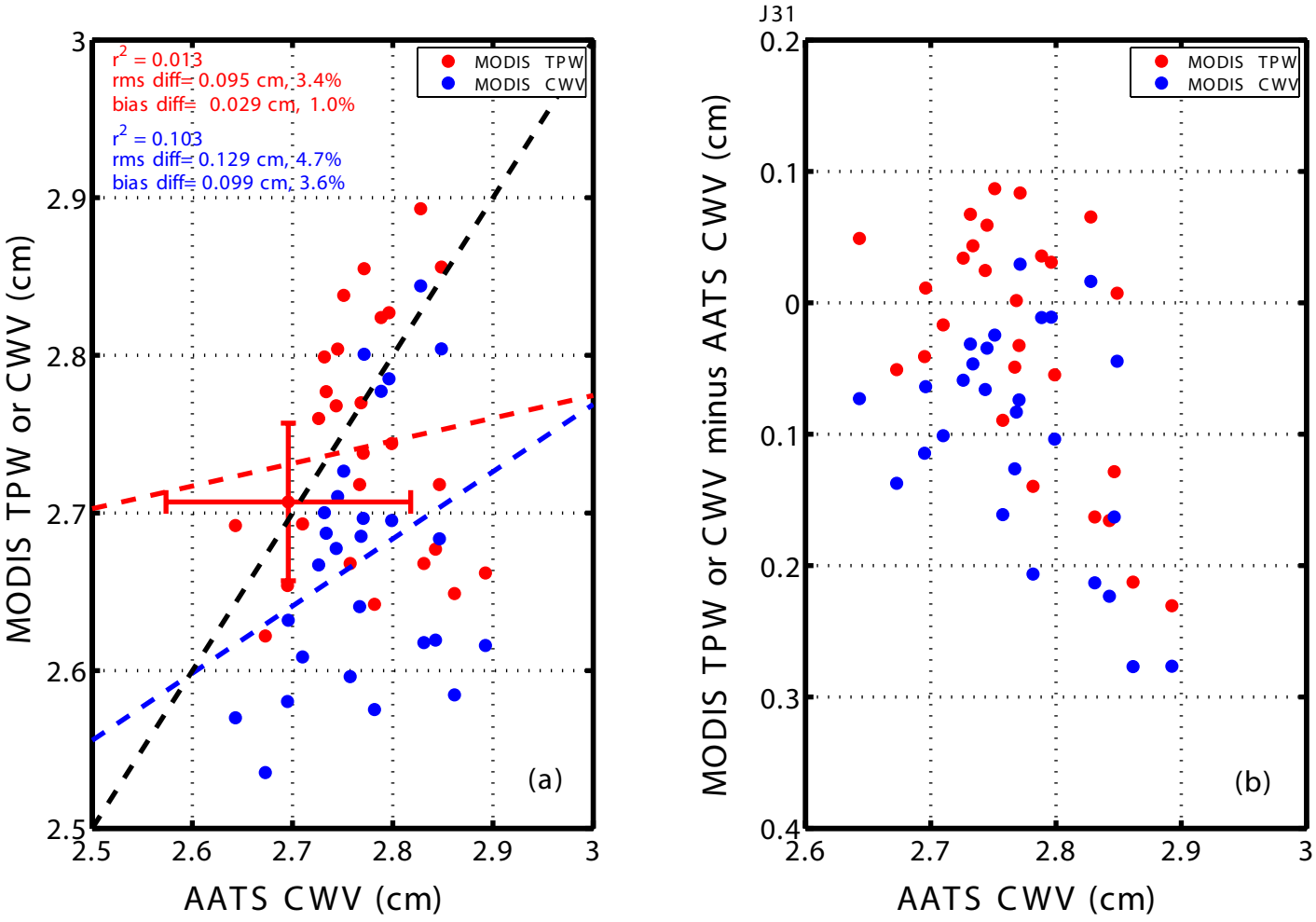

Figure 8. (a) Scatterplot of MODIS TPW and CWV versus AATS CWV. Bars show representative uncertainties. (b) MODIS TPW minus AATS CWV and MODIS CWV minus AATS CWV.

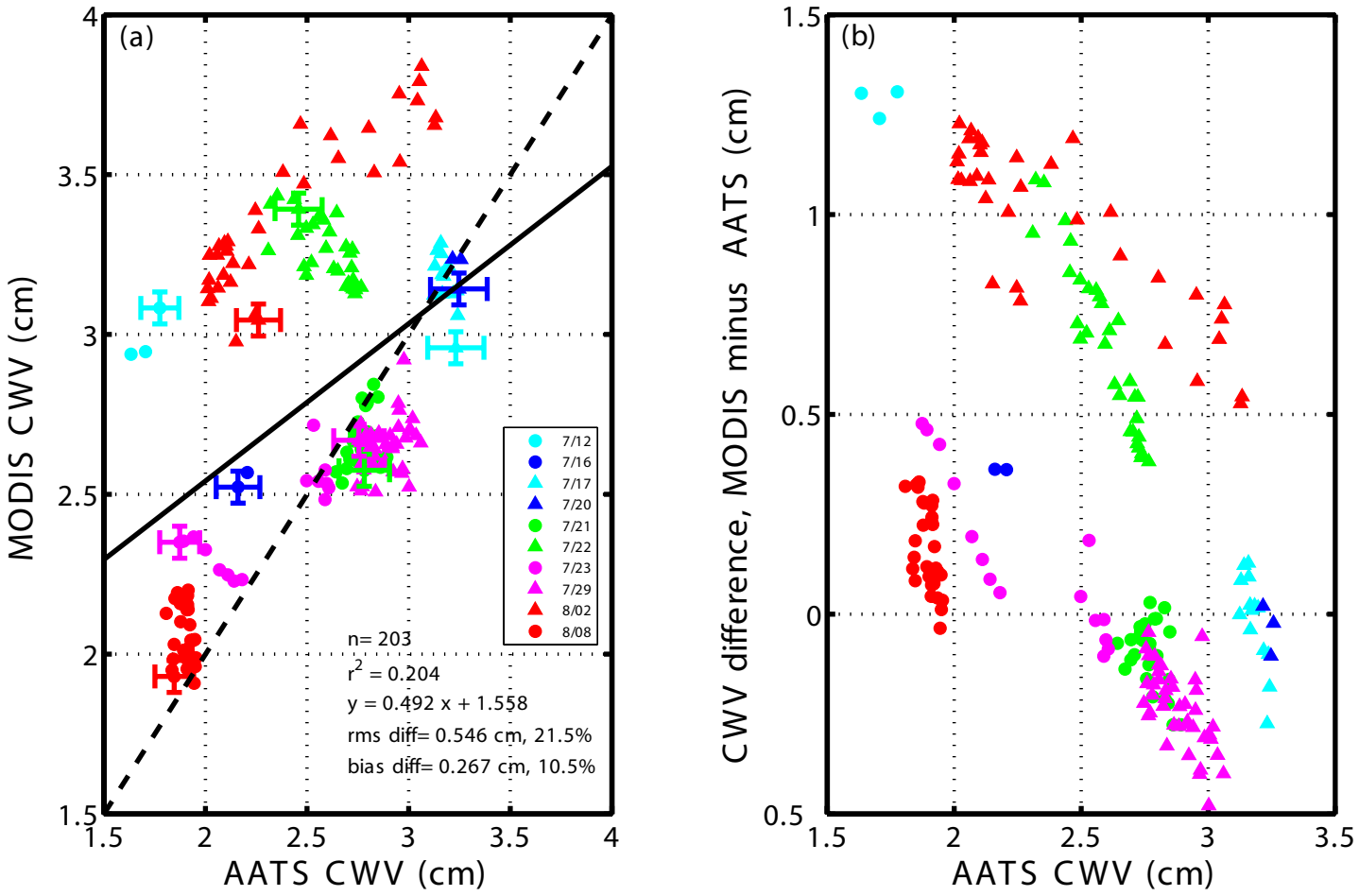

Figure 9. Comparison of MODIS IR and AATS CWV (a) retrievals and (b) differences for 203 MODIS grid cells during 5 MODIS-Aqua (solid circles) and 5 MODIS-Terra (solid triangles) overpasses.

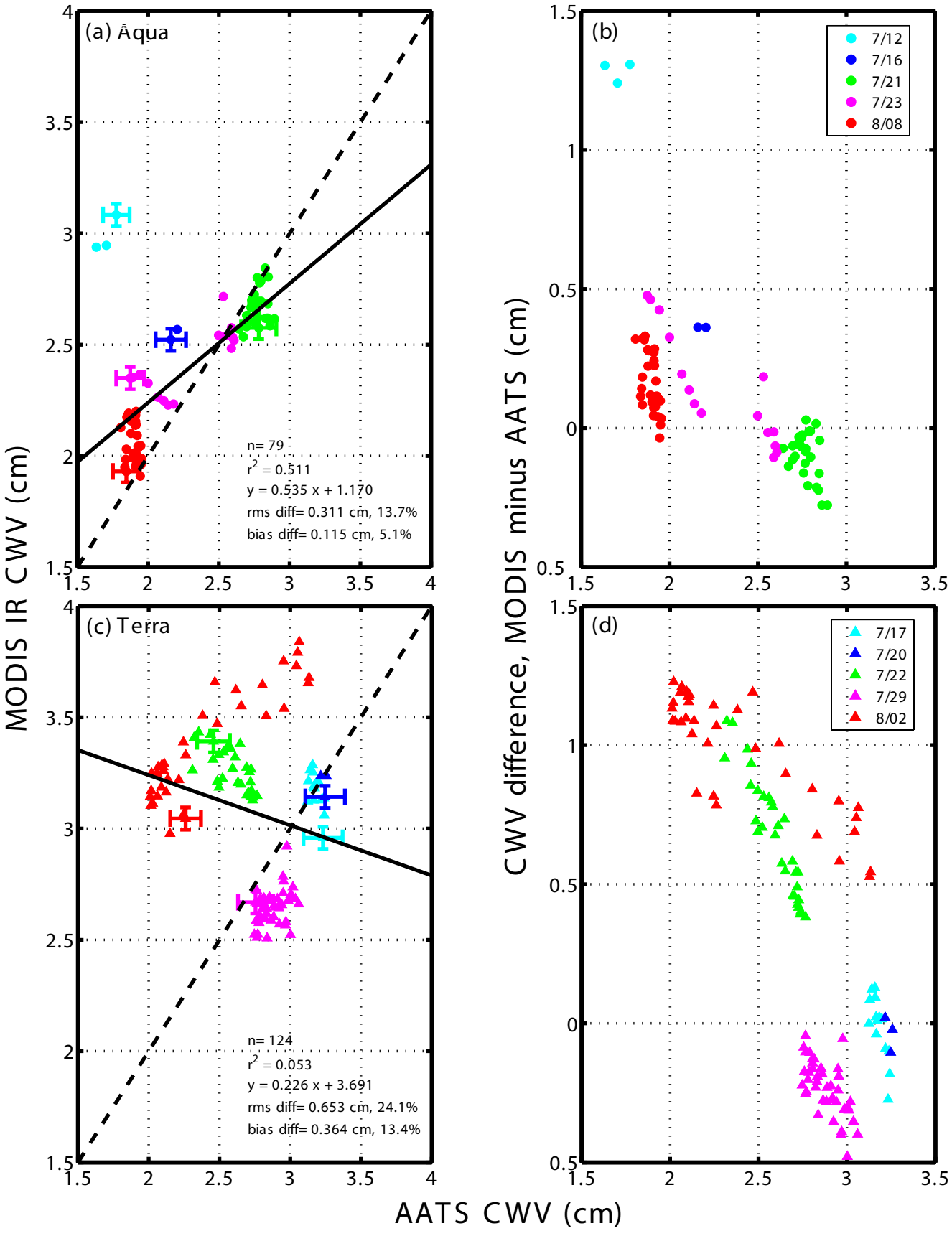

Figure 10. Same as Figure 9, but (a,b) for MODIS-Aqua comparisons only, and (c,d) for MODIS-Terra comparisons only.

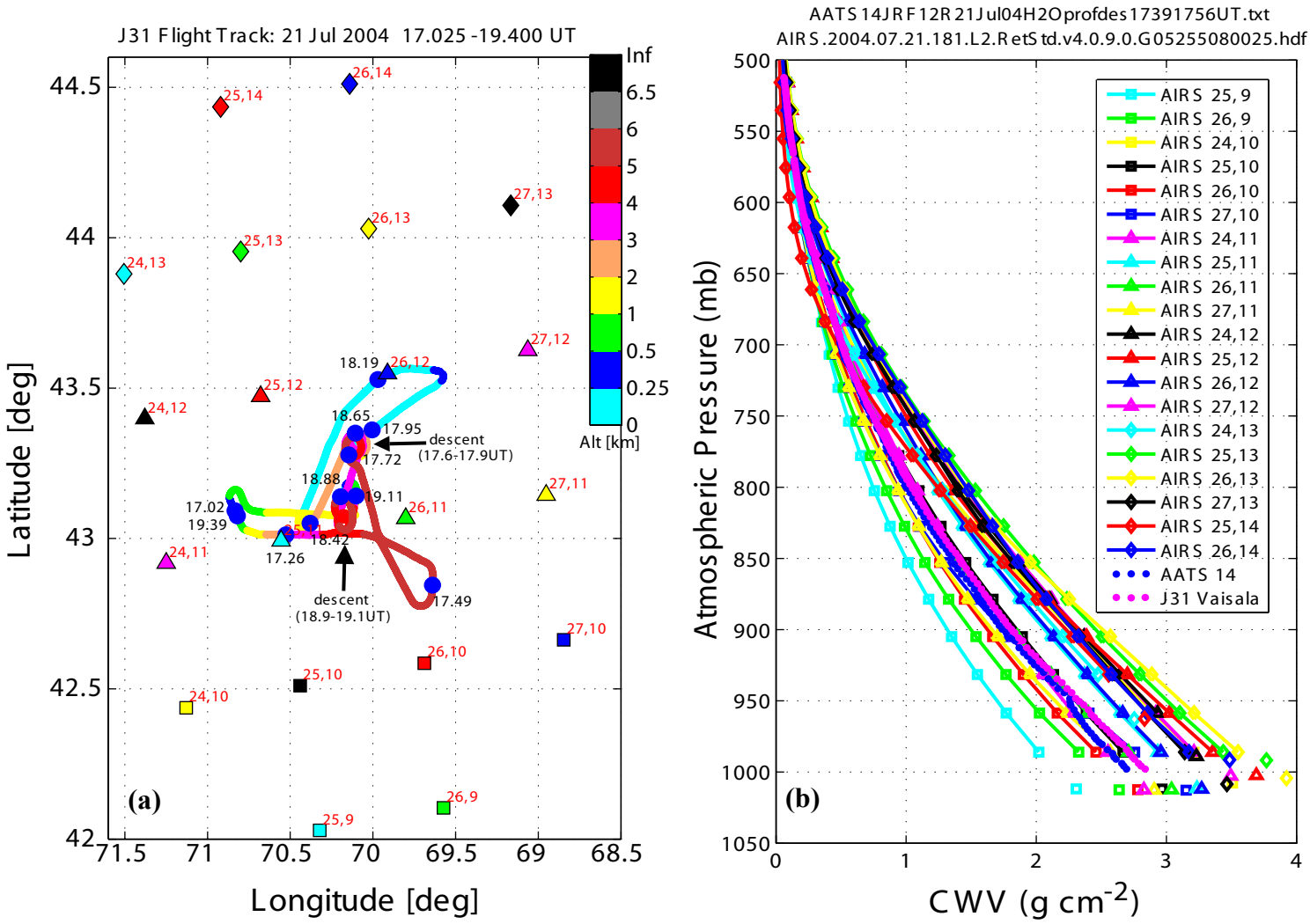

Figure 11. (a) Map view of J31 flight track (color coded by aircraft altitude) on 21 July and the center point locations of the 20 AIRS water vapor vertical profile retrievals within 150 km of the J31 17.6-17.9 UT descent (numbers in red give across-track and along-track data indices); (b) Profiles of AIRS CWV retrievals at each of the AIRS locations and AATS-14 and J31 Vaisala CWV measured during the J31 descent.

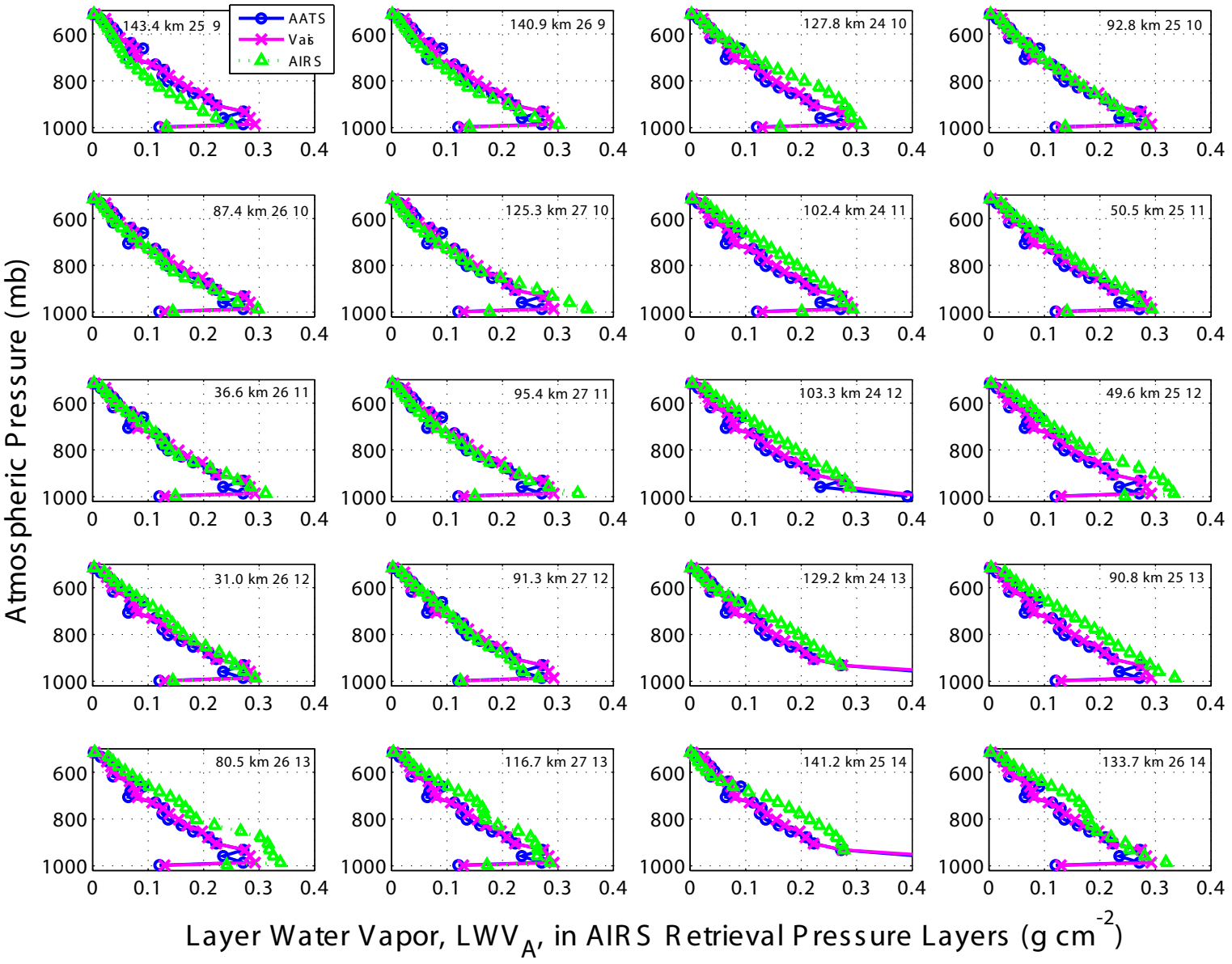

Figure 12. Profiles of AIRS, AATS-14, and J31 Vaisala LWV$_A$ retrievals within the AIRS retrieval pressure layers for the J31 1739-1756 UT descent and the AIRS profiles shown in Figure 11. Text in each frame gives the mean distance from the J31 profile to the AIRS retrieval center point, in addition to the cross-track and along-track indices of the AIRS location.

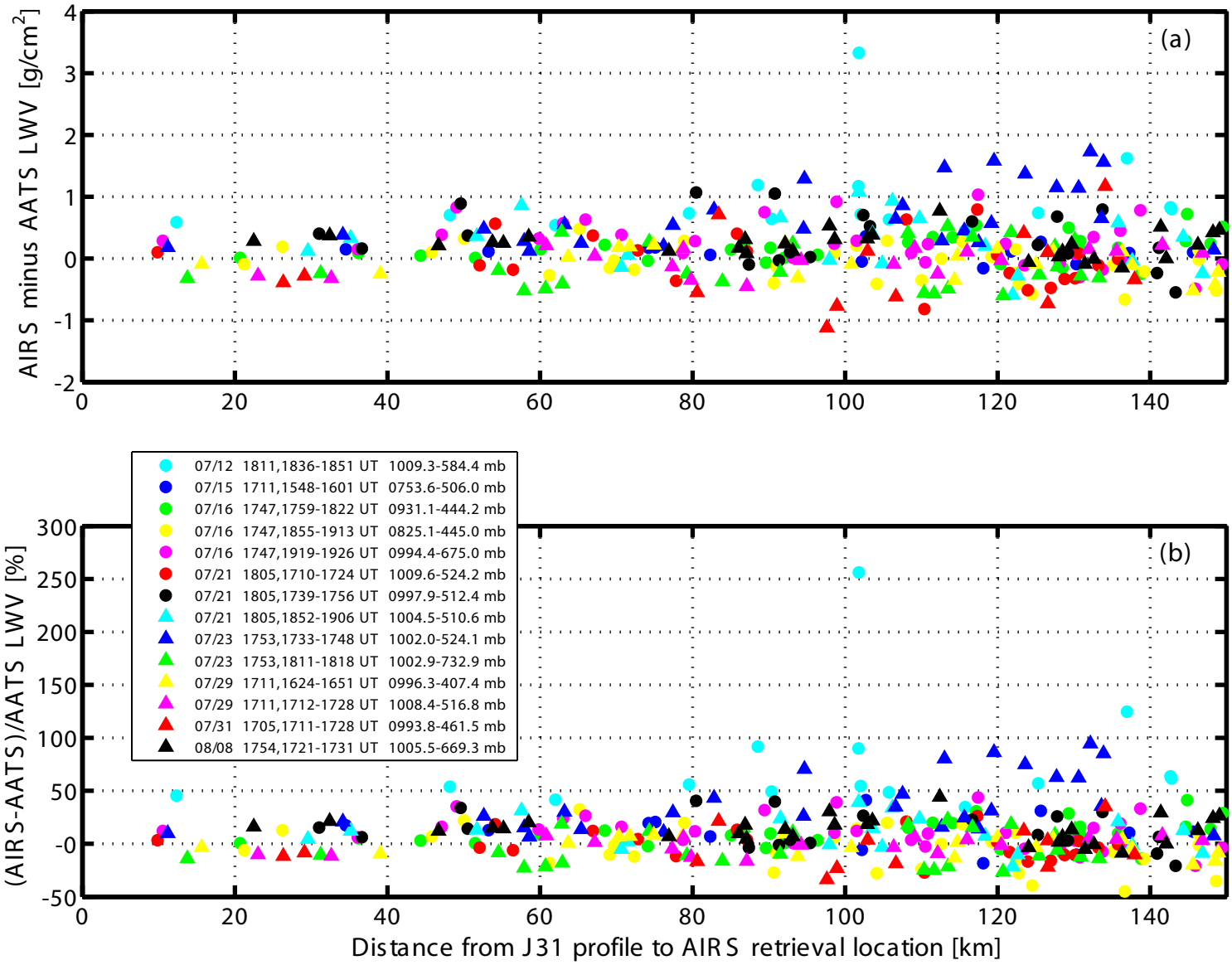

Figure 13. Dependence of AIRS minus AATS (a) absolute and (b) relative LWV differences on the distance from the AIRS retrieval location to the mean location of the appropriate J31 profile for 14 separate J31 profiles during 8 Aqua overpasses. Legend gives date, Aqua overpass time, J31 profile times, and vertical extent of each J31 profile.

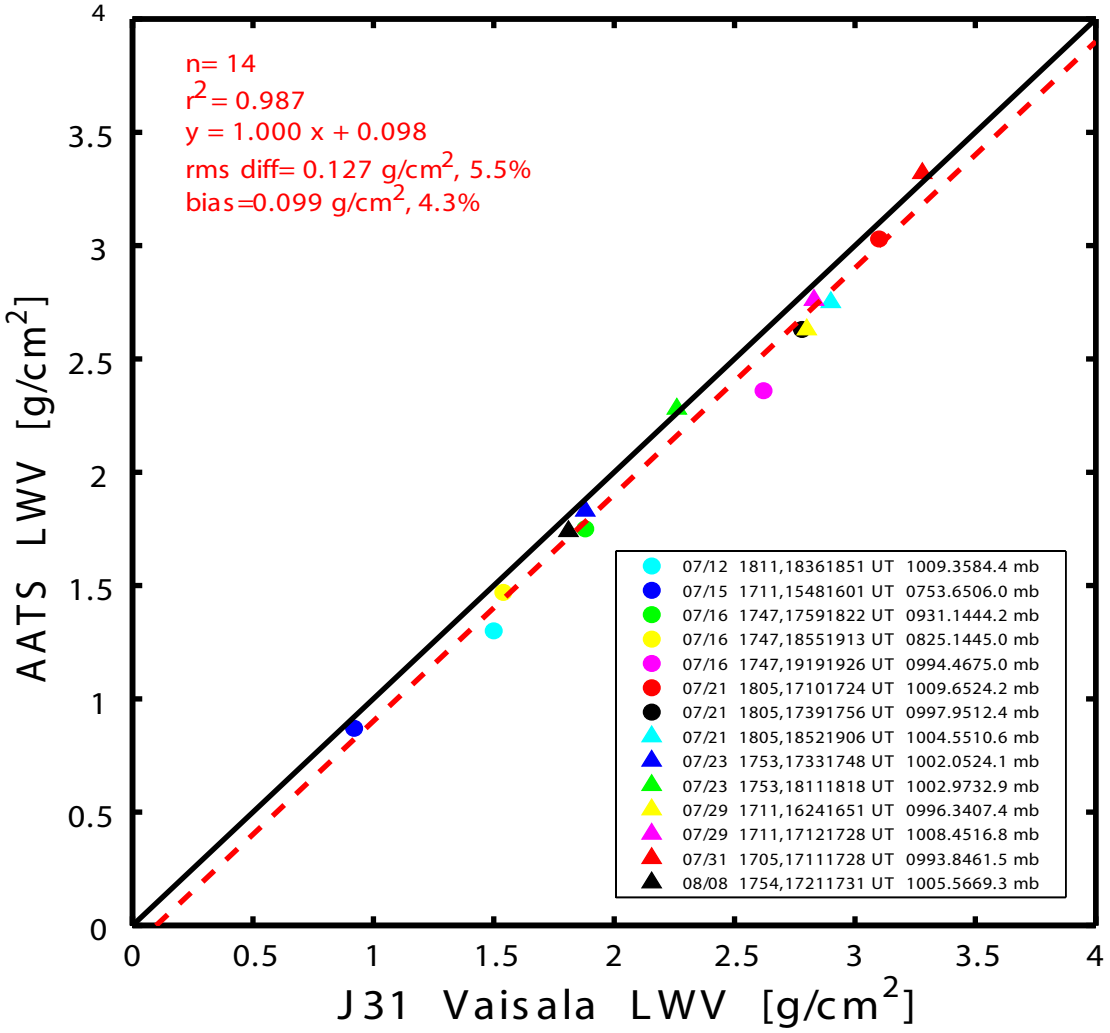

Figure 14. Comparison of AATS and J31 Vaisala LWV measurements for 14 J31 vertical profiles within 90 minutes of Aqua overflights for which AIRS retrievals of water vapor profiles are available.

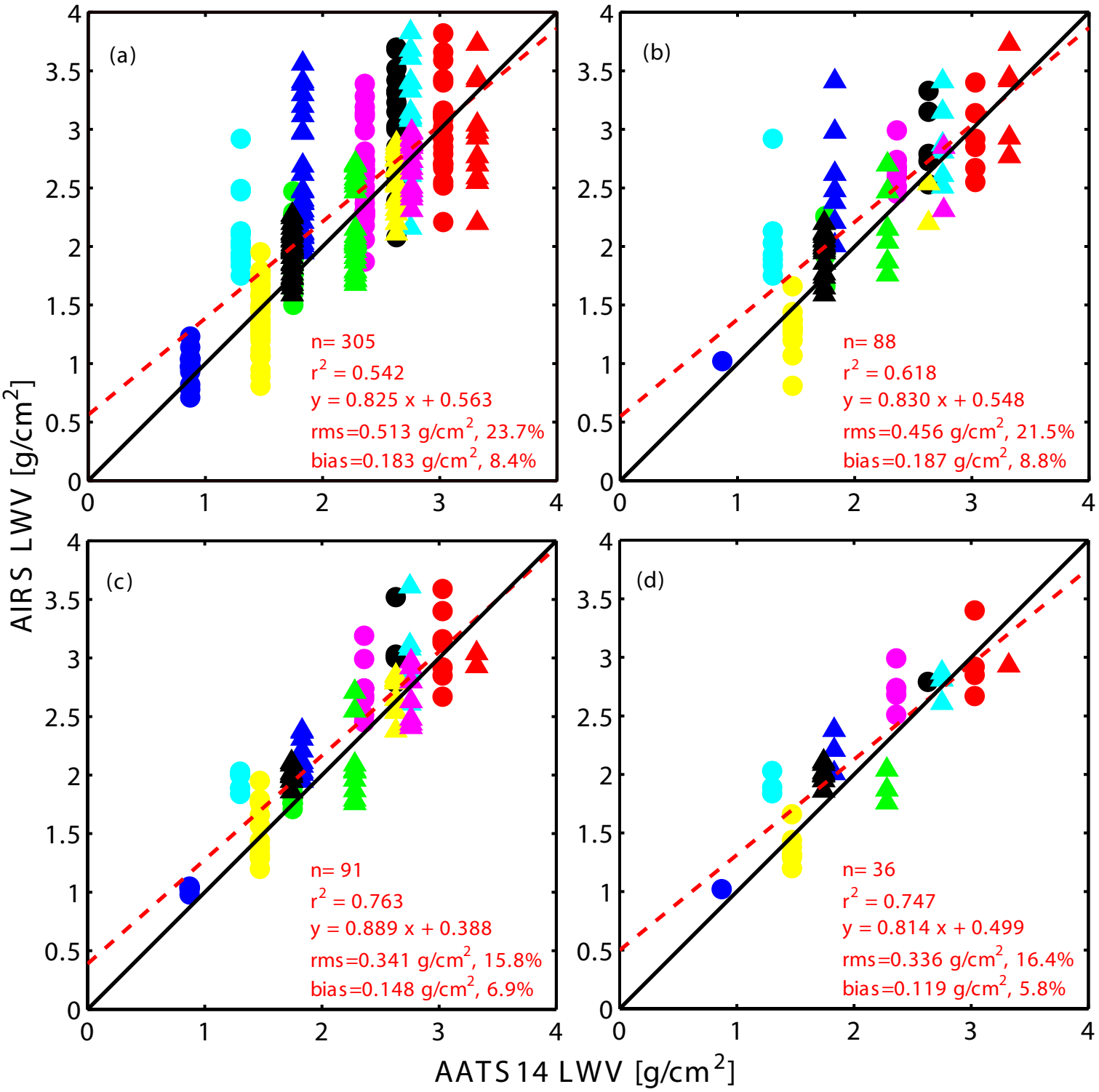

Figure 15. Scatterplot comparisons of AIRS and AATS LWV for (a) AIRS retrievals within 150 km of a J31 profile for AIRS retrieval control flag *Qual_Temp_Profile_Bot* = 2, (b) AIRS retrievals within 150 km of a J31 profile for *Qual_Temp_Profile_Bot* = 0, (c) AIRS retrievals within 80 km of a J31 profile for flag *Qual_Temp_Profile_Bot* = 2, (d) AIRS retrievals within 80 km of a J31 profile for *Qual_Temp_Profile_Bot* = 0.

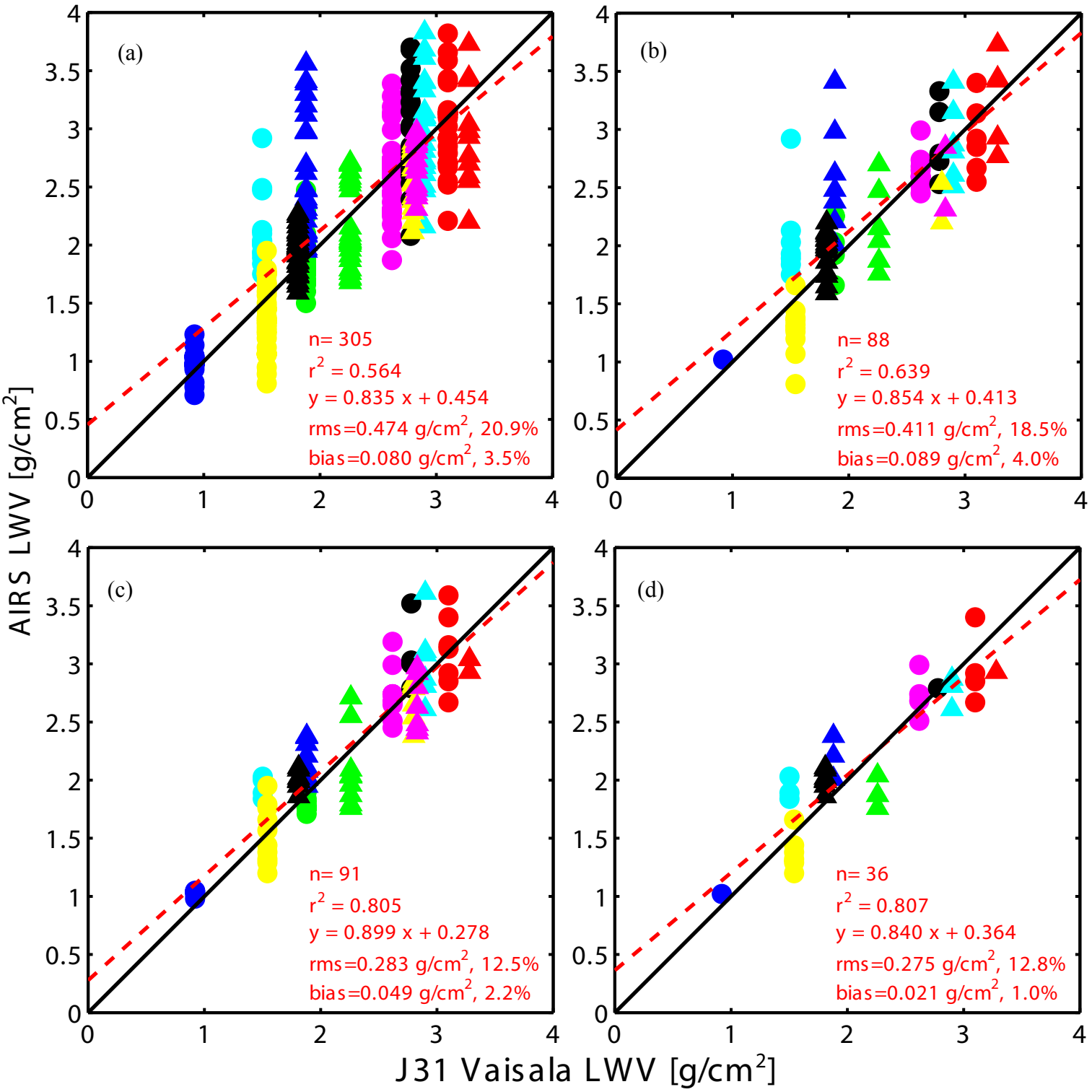

Figure 16. Scatterplot comparisons of AIRS and J31 Vaisala LWV for (a) AIRS retrievals within 150 km of a J31 profile for AIRS retrieval control flag *Qual_Temp_Profile_Bot* = 2, (b) AIRS retrievals within 150 km of a J31 profile for *Qual_Temp_Profile_Bot* = 0, (c) AIRS retrievals within 80 km of a J31 profile for flag *Qual_Temp_Profile_Bot* = 2, (d) AIRS retrievals within 80 km of a J31 profile for *Qual_Temp_Profile_Bot* = 0.

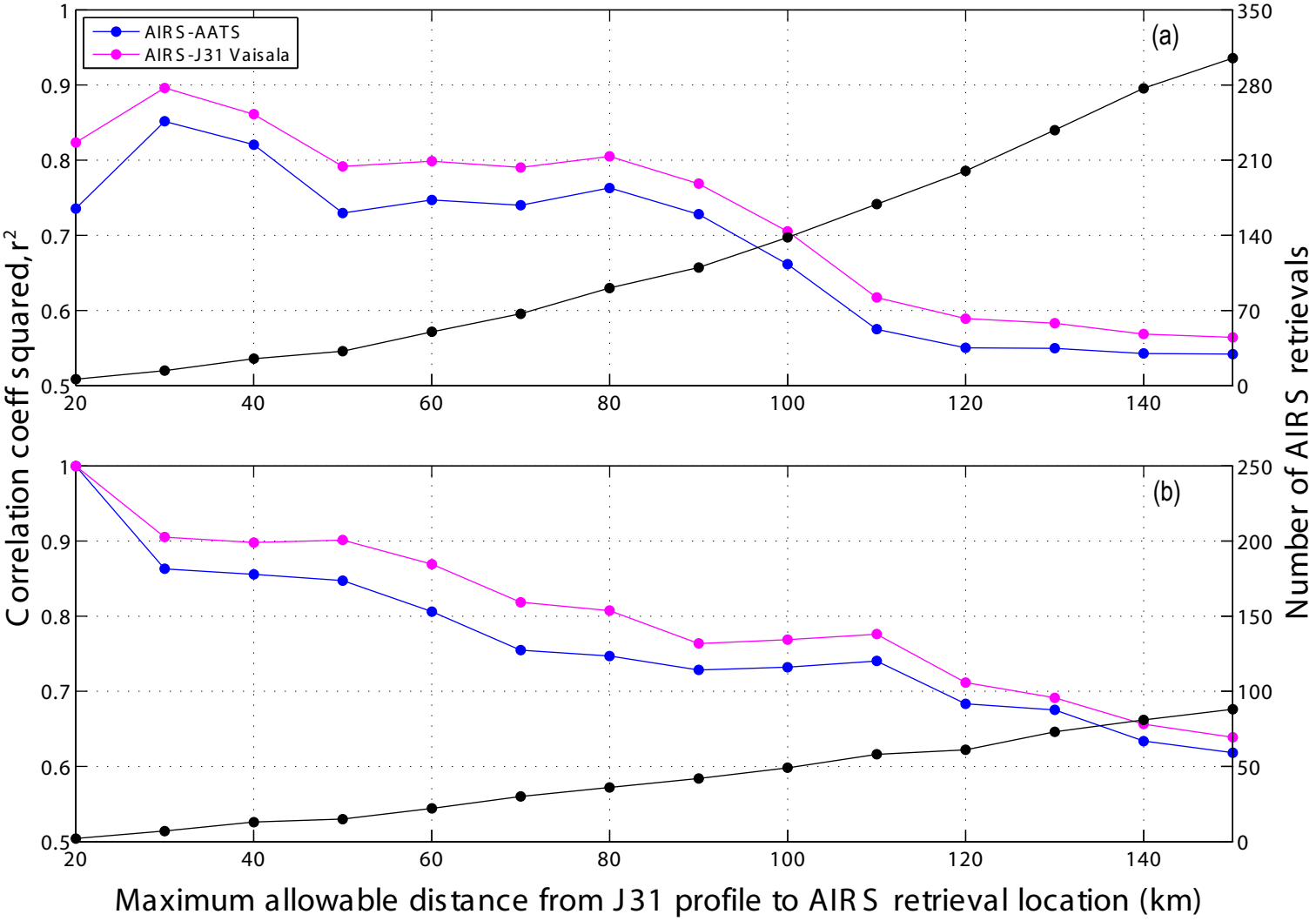

Figure 17. Variation of r^2 for AIRS-AATS and AIRS-Vaisala LWV retrievals as a function of the maximum allowable distance from the J31 profile to the AIRS retrieval location for: (a) *Qual_Temp_Profile_Bot* = 2, and (b) *Qual_Temp_Profile_Bot* = 0. The numbers of AIRS retrievals included in the analyses are also shown.

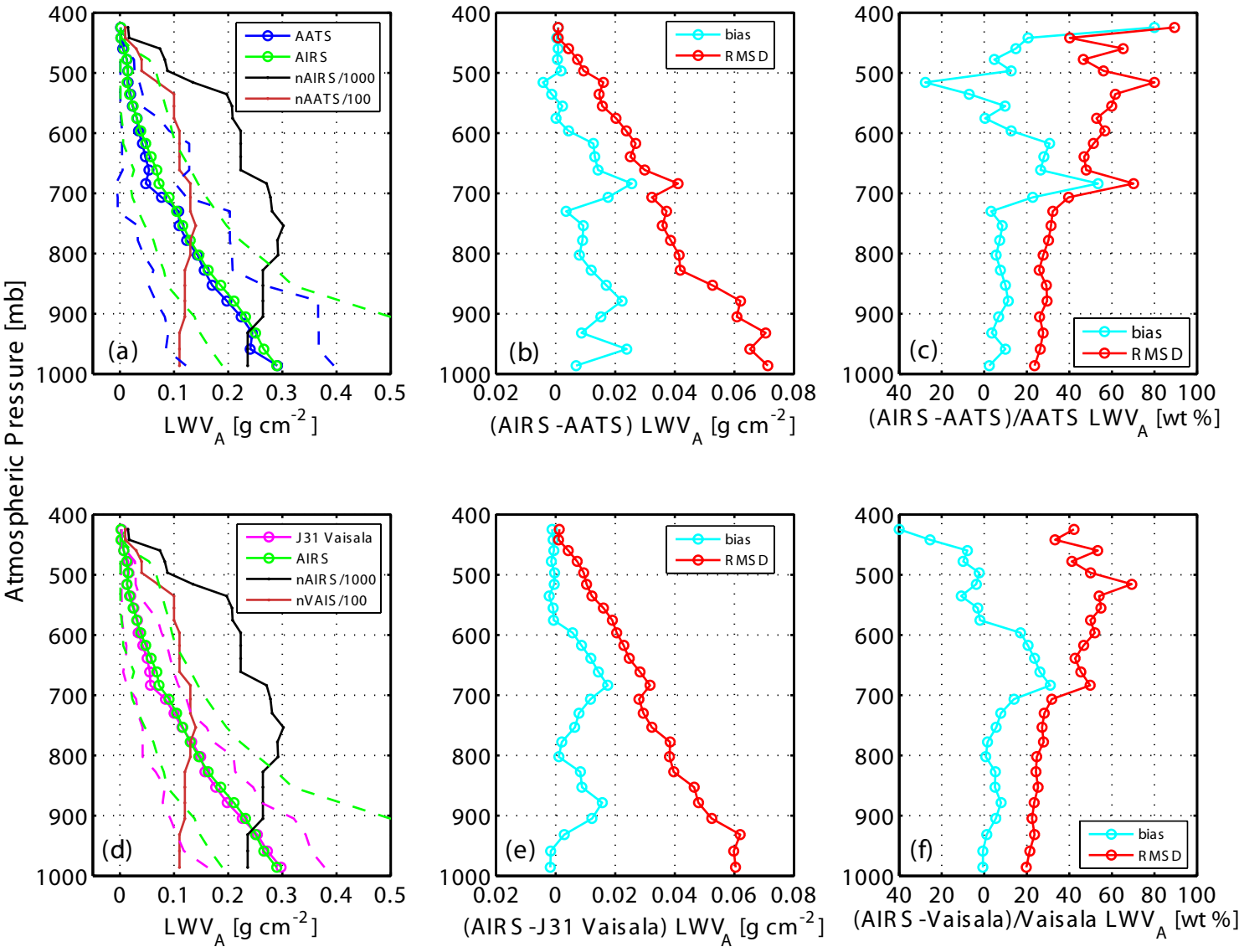

Figure 18. Results of AIRS and J31 sensor comparisons of LWV_A for AIRS retrievals with *Qual_Temp_Profile_Bot* = 2 and within 150 km of a J31 vertical profile. (a) Means (open circles with solid lines) and ranges (dashed lines) of AIRS and AATS LWV_A profile retrievals, numbers of AIRS and AATS retrievals at each altitude; (b) absolute AIRS minus AATS LWV_A biases and rms differences; (c) relative AIRS minus AATS LWV_A biases and rms differences; (d-f) same as (a-c) but for AIRS-J31 Vaisala comparisons.

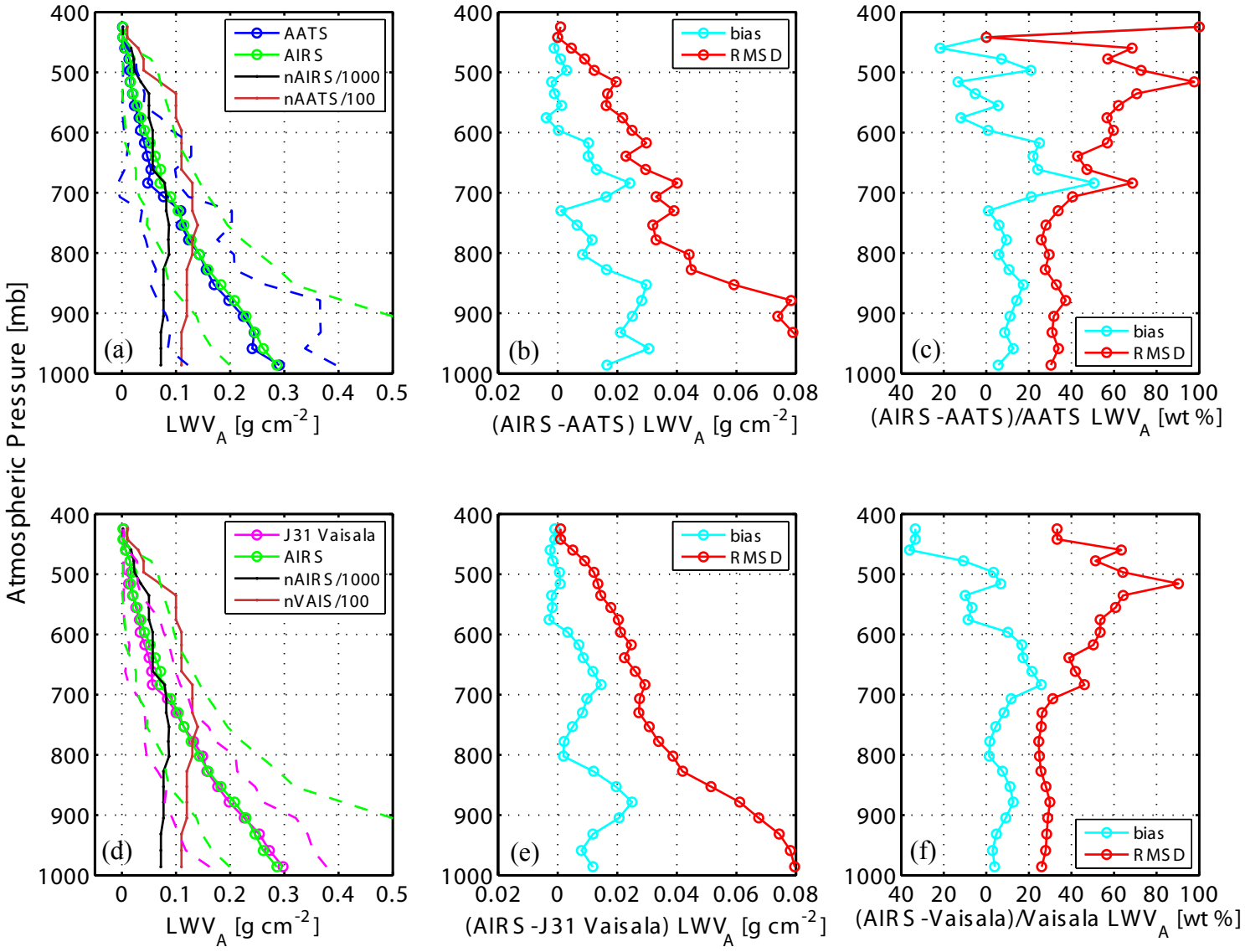

Figure 19. Same as Figure 18, but for AIRS retrievals with *Qual_Temp_Profile_Bot* = 0 and within 150 km of a J31 vertical profile.

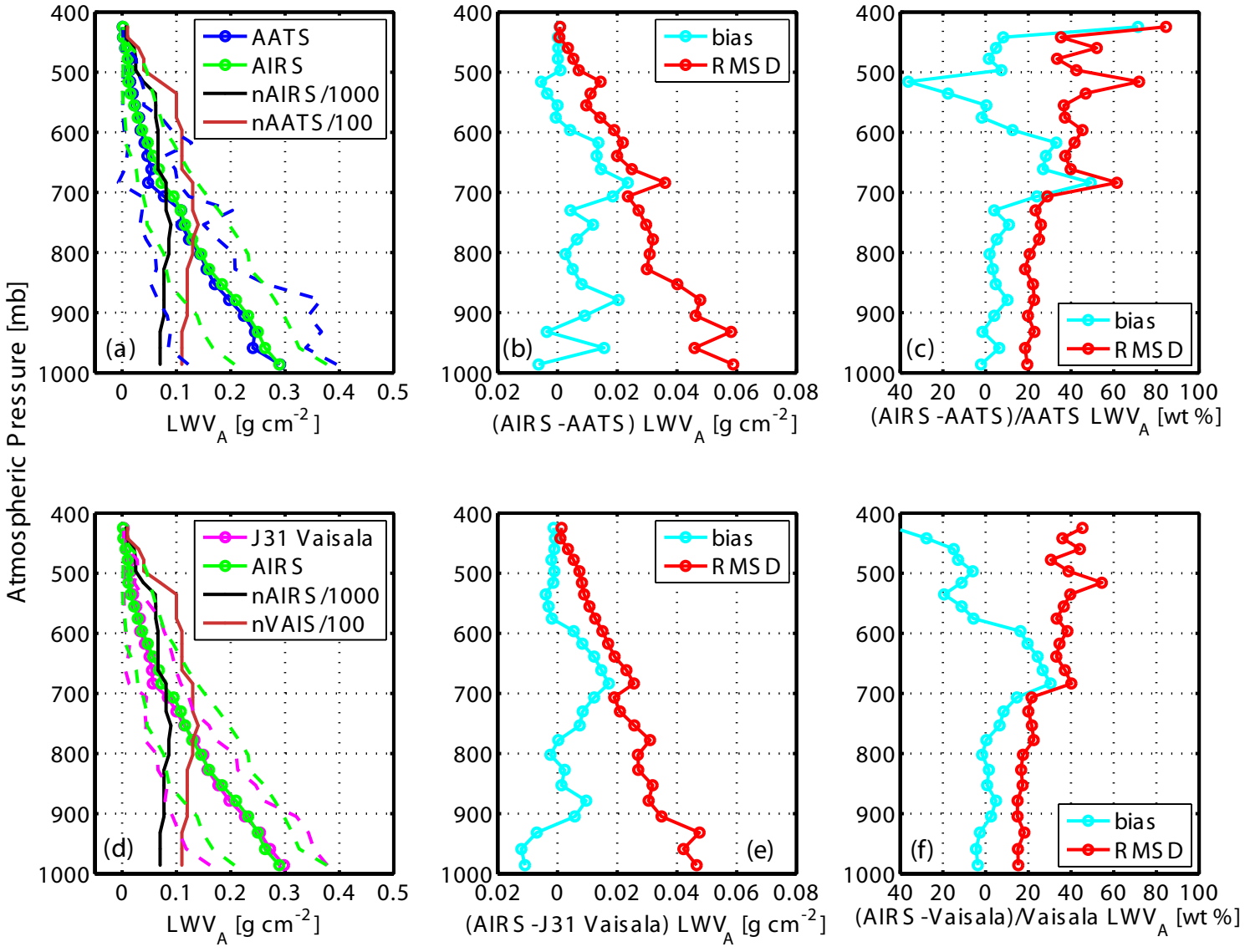

Figure 20. Same as Figure 18, but for AIRS retrievals with *Qual_Temp_Profile_Bot* = 2 and within 80 km of a J31 vertical profile.

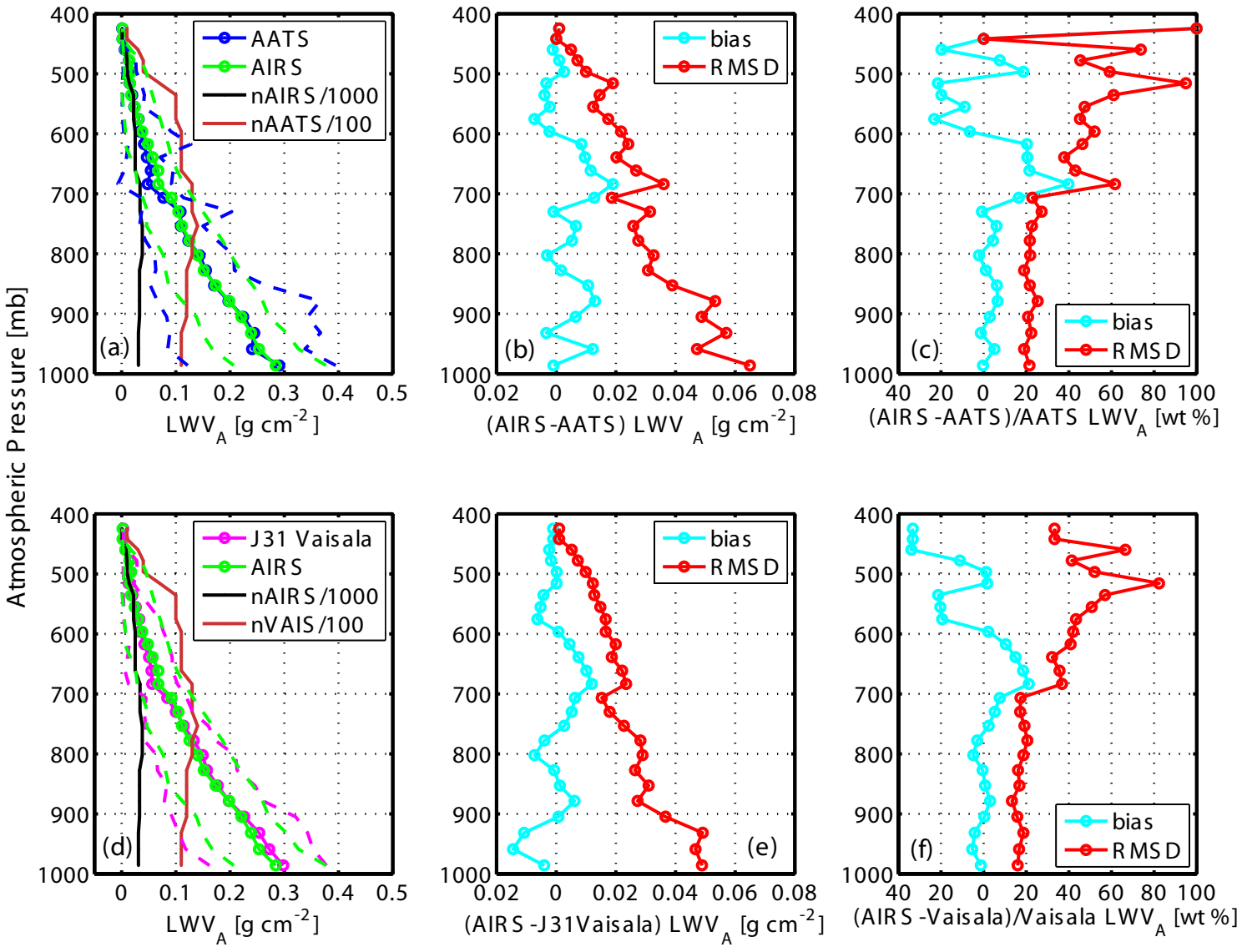

Figure 21. Same as Figure 19, but for AIRS retrievals with *Qual_Temp_Profile_Bot* = 0 and within 80 km of a J31 vertical profile.

Comparison of Water Vapor Measurements by Airborne Sunphotometer and Near-Coincident In Situ and Satellite Sensors during INTEX-ITCT 2004

J. Livingston[1], B. Schmid[2], J. Redemann[2], P. B. Russell[3], S. A. Ramirez[2], J. Eilers[3], W. Gore[3], S. Howard[2], J. Pommier[2], E. J. Fetzer[4], S. W. Seemann[5], E. Borbas[5], D. Wolfe[6]

Submitted to JGR-Atmospheres

30 June 2006

Corresponding author: John M. Livingston
SRI International
333 Ravenswood Avenue
Menlo Park, CA 94025 U.S.A.
Phone: +1 650 859 4174
Fax: +1 650 322 3218
e-mail: john.livingston@sri.com

Affiliations:

[1]SRI International, 333 Ravenswood Ave., Menlo Park, CA 94025 USA
[2]Bay Area Environmental Research Institute, 560 Third St. West, Sonoma, CA 95476 USA
[3]NASA Ames Research Center, MS 245-5, Moffett Field, CA 94035-1000 USA
[4]Jet Propulsion Laboratory, California Institute of Technology, Pasadena, CA 91109 USA
[5]University of Wisconsin – Madison, CIMSS, 1225 West Dayton Street, Madison, WI 53706 USA
[6]NOAA Earth System Research Laboratory, 325 Broadway, Boulder, CO 80305 USA

Abstract

The NASA Ames 14-channel Airborne Tracking Sunphotometer (AATS-14) took measurements from aboard a Jetstream 31 (J31) aircraft during 19 science flights over the Gulf of Maine in support of the 2004 field studies INTEX-NA (INtercontinental chemical Transport EXperiment-North America) and ITCT (Intercontinental Transport and Chemical Transformation of anthropogenic pollution). We use AATS-14 retrievals of columnar water vapor (CWV) obtained during aircraft vertical profiles to compare layer-integrated (over the altitude range traversed during the vertical profile) water vapor (LWV) and water vapor density (ρ_w) with simultaneous measurements obtained with an onboard Vaisala HMP243 humidity sensor and with spatially and temporally near-coincident measurements from radiosondes launched from the NOAA R/V Ronald H. Brown. We compare AATS CWV measurements acquired during low level (typically 60-120 m ASL) aircraft transects over the ocean with MODIS infrared (IR) retrievals of CWV in 203 MODIS grid cells (5 x 5-km resolution at nadir) during 5 Aqua and 5 Terra overpasses. We also compare AIRS water vapor profile retrievals acquired during 8 Aqua overpasses with corresponding J31 AATS and Vaisala retrievals obtained during 14 aircraft vertical profiles within ~1.5 hr of satellite overpass. We calculate AIRS LWV for direct comparison with the J31 measurements of LWV, and we interpolate within the J31 AATS and Vaisala water vapor retrievals to calculate the amount of water vapor, LWV_A, within the layers defined by the AIRS pressure levels for which J31 data are available. The quality of the AIRS-J31 LWV and LWV_A comparisons is examined with respect to AIRS data quality flags and the distance from the AIRS retrieval to the J31 vertical profile.

1. Introduction

During July and August 2004, a twin turboprop Jetstream 31 (J31) flew 19 science flights over the Gulf of Maine in support of the International Consortium for Atmospheric Research on Transport and Transformation [ICARTT, *Fehsenfeld et al.*, 2006] effort to quantify the air quality, intercontinental transport, and radiative energy budgets in air masses moving across the US and over the Atlantic Ocean to Europe. ICARTT included Phase A of the Intercontinental Chemical Transport Experiment [INTEX-A, *Singh et al.*, 2006] and the Intercontinental Transport and Chemical Transformation (ITCT) experiment. The goal of the J31 flights was to characterize aerosol, water vapor, cloud, and ocean surface radiative properties and effects in flights that sampled polluted and clean air masses in coordination with measurements from other aircraft, a ship, and various satellites. Specific science objectives of the J31 included validating satellite retrievals of aerosol optical depth (AOD) spectra and of water vapor columns, as well as measuring aerosol effects on radiative energy fluxes.

The primary instruments on the J31 were the 14-channel NASA Ames Airborne Tracking Sunphotometer (AATS-14) and an upward- and downward-looking pair of solar spectral flux radiometers. Other instrumentation included a Vaisala HMP243 humidity sensor and other instruments to provide basic meteorological and navigational information. J31 flight patterns included a mixture of vertical profiles (spiral and ramped ascents and descents) and constant altitude horizontal transects at a variety of altitudes. In most cases, flights were designed to include a near sea surface horizontal transect in a region of minimal cloud cover during or near the time of an Aqua and/or Terra satellite overpass, in addition to a low altitude flyby and vertical profile above the NOAA ship Ronald H. Brown. AATS-14 measurements of the direct

beam solar transmission allow retrieval of instantaneous aerosol optical depth (AOD) at 13 wavelengths and columnar water vapor (CWV). Data obtained during suitable aircraft ascents and descents can be differentiated to yield vertical profiles of aerosol extinction and water vapor density (ρ_w).

Because water vapor is the primary gaseous absorber of infrared radiation in the atmosphere, knowledge of its horizontal and vertical distribution is critical to understanding its effect on the Earth's climate. Fortunately, continuous global measurements of the distribution of water vapor are now being acquired by satellite sensors such as the Moderate Resolution Imaging Spectroradiometer (MODIS, *Kaufman et al.*, 1997) on Aqua and Terra, the Atmospheric Infrared Sounder (AIRS, *Aumann et al.*, 2003) instrument suite on Aqua, and the Tropospheric Emission Spectrometer (TES, *Beer*, 2006) on Aura. While only satellite sensors can provide a global view, there remains a critical need for continuing validation of the satellite products by information from sensors with superior measurement capabilities. Existing international networks of radiosondes and ground-based sunphotometers (AERONET, *Holben et al.*, 1998), and lidars and microwave radiometers at selected land sites (e.g., the Atmospheric Radiation Measurement Southern Great Plains [ARM-SGP] site) are available and can be used to validate satellite water vapor retrievals over land [e.g., *Whiteman et al.*, 2006; *Tobin et al.*, 2006]. However, validation of satellite over-ocean water vapor retrieval algorithms generally must rely on a combination of sparse radiosonde or remote measurements and numerical model outputs. This is a role for which AATS-14 and the J31 are well-suited. Previous studies [*Schmid et al.*, 2000, 2003a, 2006] have compared AATS-14 retrievals of CWV and water vapor density over land and over ocean with coincident aircraft-based in-situ and/or ground-based remote

measurements. This paper compares AATS-14 over-ocean water vapor retrievals with simultaneous in-situ water vapor measurements by the J31 Vaisala sensor and with temporally and spatially near-coincident measurements from radiosondes released from the Ron Brown, and it extends the comparisons to corresponding water vapor retrievals by MODIS and by AIRS. In other papers dealing with AATS-14 measurements acquired during INTEX/ITCT, *Russell et al*. [2006] discuss the AATS-14 AOD measurements and comparisons to MODIS and to MISR (Multiangle Imaging SpectroRadiometer, *Diner et al.*, 1998, *Martonchik et al.*, 1998), *Redemann et al.* [2006] present the J31 measurements of aerosol effects on radiative energy fluxes, and *Pilewskie et al.* [2006] report cloud properties derived from J31 measurements of visible and near-infrared reflectance in the presence of aerosols.

2. Data Sources

2.1 Airborne sunphotometer

The NASA Ames Airborne Tracking Sunphotometer (AATS-14) measures the (relative) intensity of the direct solar beam in 14 spectral channels with center wavelengths ranging from 354 to 2138 nm and full width at half maximum (FWHM) bandwidths of ~5 nm (exceptions are 2.0 nm for the 354-nm channel and 17.3 nm for the 2138-nm channel). The data acquisition system samples at three Hz, and every four seconds it records detector voltages consisting of an average and standard deviation of nine samples taken during the first three of the four seconds. These data are stored together with data on instrument tracking and temperature control, aircraft location, and ambient temperature, relative humidity, and static pressure. The standard deviations of all channels are used subsequently in a cloud-screening algorithm, as described by *Schmid et al.* [2003b]. Data are transmitted serially from a computer within the instrument to a

remote operator station (laptop computer). The science data are then combined with previously determined radiometric calibration values to calculate and display aerosol optical depth (AOD, $\tau_p(\lambda)$) and columnar water vapor (CWV) in real time at the operator station. For more information on the instrument and its mounting on the J31, see the companion paper by *Russell et al.* [2006].

Our methods for data reduction, calibration, and error analysis have been described in detail previously (*Russell et al.*, 1993a, 1993b; *Schmid and Wehrli*, 1995; *Schmid et al.*, 1996, 1998, 2001, 2003b). The AATS-14 channels have been chosen to permit separation of total (path-integrated) aerosol, water vapor, and (under suitable conditions) ozone attenuation along the slant path from the sun to the instrument. In practice, the measured detector voltages are combined with separately determined (see following paragraph) exoatmospheric detector voltages, $V_0(\lambda)$, to yield slant-path transmissions. From these slant-path transmissions we retrieve $\tau_p(\lambda)$ in 13 narrow wavelength bands centered between 354 and 2139 nm and columnar water vapor from the channel centered at 941 nm. For measurements acquired during INTEX/ITCT, we use ozone total column amounts from TOMS satellite retrievals and adjust these values for the J31 altitude using the 1976 standard ozone model vertical distribution. Rayleigh scattering corrections use the *Bucholtz* [1995] cross sections and static pressure measured on the J31. As described by *Russell et al.* [2006], measurements in some AATS-14 channels also require corrections for gas absorption (NO_2, H_2O, O_2-O_2, CH_4, N_2O, and CO_2) in order to retrieve AOD.

AATS was calibrated by analysis of sunrise measurements acquired at Mauna Loa Observatory (MLO), Hawaii, in June 2004 before the ITCT deployment and also by analysis of sunset measurements acquired on four dedicated J31 flights during the experiment. Exoatmospheric detector voltages, $V_0(\lambda)$, were derived using the Langley plot technique (e.g., *Russell et al.*, 1993a, 1993b; *Schmid and Wehrli*, 1995) for all channels except 941 nm, for which a modified Langley technique was employed to account for water vapor absorption [*Reagan et al.*, 1995; *Michalsky et al.*, 1995; *Schmid et al.*, 1996, 2001]. Mean values of $V_0(\lambda)$ obtained during the four ITCT calibration flights agreed with the pre-mission MLO mean values to ≤0.5% in all channels except 519 nm and 1240 nm, where differences were 0.7% and 1.3%, respectively. In the 941-nm channel, mean values agreed to within 0.4%. For all channels except 941 nm, standard deviations in the calculated V_0 values ranged from <0.1% to 0.3% for the MLO measurements, and from <0.1% to 0.8% for the airborne measurements. Corresponding standard deviations in V_0 in the 941-nm channel were 1.8% for the MLO data and 1.1% for the airborne measurements. Resulting uncertainties in derived CWV due to the uncertainty in V_0 are included in the error bars shown in various figures in this paper.

Because absorption by water vapor varies strongly within the 5-nm FWHM bandpass of the AATS-14 channel centered at 941 nm, the usual Beer-Lambert-Bouguer expression must be modified to describe correctly the relationship between the incoming directly transmitted solar irradiance and the output detector voltage, V(941), within that channel. In particular,

$$V(941\ \text{nm}) = V_0(941\ \text{nm})\, d^{-2} \exp\left[-\sum_i m_i \tau_i(941nm) \right] T_w, \qquad (1)$$

where $V_0(941\ \text{nm})$ is the exoatmospheric voltage constant, d is the Earth-Sun distance in astronomical units at the time of observation, $\tau_i(941\ \text{nm})$ is the spectral optical depth due to

aerosol extinction, Rayleigh scattering, or ozone absorption, and T_w is the band- and source-weighted water vapor transmittance. In our analysis of the AATS-14 INTEX/ITCT data set, we employed an expression analogous to that of the three-parameter expression of *Ingold et al.* [2000] for parameterizing the water vapor transmittance, T_w:

$$T_w = c \exp(-aw_s b), \quad (2)$$

where w_s is the amount of water vapor along the slant path and is in units of g/cm^2 (or typical precipitable water vapor units of cm, since the mean liquid water density = 1 g/cm^3), and the coefficients a, b and c are least squares fitting parameters determined by executing a radiative transfer model over a range of slant path water vapor amounts. For c=1, Eq. (2) is equivalent to the two-parameter expression of *Bruegge et al.* [1992]. Strictly speaking, as noted by *Ingold et al*. [2000], this equation only applies for $w_s > 0$ to avoid the nonphysical result for $c \neq 1$ at vanishing water vapor absorption ($w_s = 0$).

In practice, we applied the two- and three-parameter expressions separately to results from LBLRTM_V9.2 [*Clough et al.*, 2005] runs for a wide range of solar zenith angles (i.e., airmasses) and the 6 built-in standard atmospheres at aircraft (AATS) altitudes every 1 km between the surface and 8 km. Results for the two- and three-parameter fits were quite close below 4 km, so we used the two-parameter fits at altitudes 0-3 km, and the 3-parameter fits at altitudes 4-8 km. The results for altitudes ≤6 km are shown in Figure 1 for slant water paths measured during INTEX-ITCT, and the fitting coefficients are listed in Table 1. Figure 1 shows that a calculation of CWV that ignores the instrument altitude can result in an incorrect

determination of slant path (hence, columnar) water vapor. In particular, if it is assumed that the instrument is located at sea level, then CWV would be underestimated for altitudes above sea level, and the errors would be greatest for large solar zenith angles (high airmass values), SZA, and high CWV (hence, high slant water vapor) amounts. For most data presented in this paper, SZA≤40°, corresponding to airmass values ≤1.3. As will be shown in Figure 2 below, typical CWV values measured by AATS during ITCT at aircraft altitudes of 1 km and 2 km were 1.0-2.0 g/cm^2 and 0.5-1.0 g/cm^2, respectively. For these CWV amounts and aircraft altitudes and for an airmass of 1.3, the errors in calculated CWV that would result from not accounting for the altitude of the measurement are ~0.06-0.14 g/cm^2 (6-7%) at 1 km and ~0.05-0.12 g/cm^2 (11-12%) at 2 km. At higher altitudes absolute errors would decrease (and relative errors would increase) because the amount of CWV above the aircraft decreases rapidly with altitude within the first few km above the surface. This altitude-dependent parameterization of water vapor transmittance as a function of slant water vapor amount represents a more realistic and rigorous treatment of airborne measurements than the single altitude parameterization that we have used in previous studies [e.g., *Schmid et al.*, 2003b; *Redemann et al*., 2003], for which it was assumed that the uncertainty in AATS CWV due to the single altitude parameterization was 0.1 g/cm^2.

Using the water vapor transmittance parameterization described above, we calculated CWV from the AATS solar transmittance measurements in the 941-nm channel. Vertical differentiation of the CWV measurements acquired during aircraft ascent or descent then yields a profile of ρ_w. In practice, we used the smoothing methodology of *Schmid et al.* [2000] to calculate ρ_w. This involves averaging the CWV profile within thin altitude bins (we used 20-50 m bins for this study), then fitting a smoothing spline to the averaged profile, and finally differentiating the

spline fit. It is necessary to smooth the CWV profile before differentiation to eliminate AATS-measured increases in CWV with height. Such increases are not possible in a horizontally homogeneous, time-invariant atmosphere. However, as noted by *Schmid et al.* [2003a], in the real atmosphere they can occur because (1) the sunphotometer can only measure the transmittance along the sunphotometer-to-sun path, (2) that path in general passes through a horizontally inhomogeneous, time-varying atmosphere, and (3) the path and the atmosphere move with respect to each other due to aircraft movement and horizontal advection. To avoid over-smoothing at altitudes that exhibit real variations of CWV we occasionally allow the water vapor density to become slightly negative. The uncertainty in CWV was computed following Schmid et al. [1996]**.** In addition, we used the method of *Schmid et al.* [2003a] to estimate the uncertainty in retrieved CWV and ρ_w due to spatial variation in CWV along the J31 flight track during the profile.

2.2 J31 Vaisala Humidity Sensor

Relative humidity was measured by a Vaisala HUMICAP Dewpoint Transmitter HMP243, which consists of two probes, a heated composite humidity HUMICAP sensor and an optional temperature head, that were mounted beneath the cockpit on the lower right side of the J31 fuselage. Total and static atmospheric pressure were measured by separate Setra Model 470 pressure sensors mounted on the J31. Prior to the ITCT deployment, both pressure sensors were calibrated in the laboratory at NASA Ames.

Both Vaisala sensor probes mounted on the J31 are subject to dynamic heating effects due to the motion of the aircraft. The static temperature, T_{static}, of the ambient atmosphere is calculated from the output, T_{total}, of the Vaisala temperature probe by

$$T_{static} = T_{total}\left(\frac{P_{static}}{P_{total}}\right)^{\left(\frac{k-1}{k}\right)}, \quad (3)$$

where $k = 1.4$ is the ratio of specific heats for water vapor, $\left(\frac{c_p}{c_v}\right)$. The quantity, $RH_{Vaisala}$, output by the Vaisala humidity sensor can be written as

$$RH_{Vaisala} = 100 * \left(\frac{e_{true}}{e_{sat}(T_{total})}\right), \quad (4)$$

where e_{true} is the true water vapor pressure, and $e_{sat}(T_{total})$ is the saturation vapor pressure at temperature T_{total}. It follows that the true ambient relative humidity is just

$$RH_{true} = RH_{Vaisala} * \left(\frac{e_{sat}(T_{total})}{e_{sat}(T_{static})}\right), \quad (5)$$

where the saturation vapor pressures at temperatures T_{total} and T_{static} are calculated using the formulae provided in the Vaisala instrument manual. The measured profiles of relative humidity, temperature, and pressure obtained during J31 ascents and descents have been converted to corresponding profiles of water vapor density using the approximate equation of

Bögel [1977]. Integration of these profiles yields the amount of water vapor (LWV) in the layer between the bottom and the top of the J31 profile.

2.3 Ship Radiosonde and Ozonesonde

Vaisala (RS92 SGP) radiosondes were launched regularly from the NOAA R/V Ronald H. Brown during summer 2004 in support of the combined NEAQS (New England Air Quality Study)-ITCT 2004 study. In addition, Vaisala (RS80) ozonesondes were also released less frequently from the Ron Brown in support of the INTEX Ozonesonde Network Study [*Thompson et al*., 2005]. The measured profiles of relative humidity, temperature, and pressure have been converted to corresponding profiles of water vapor density using *Bögel* [1977]. Integration of these profiles yields the amount of water vapor in the column (layer) bounded by the upper and lower altitudes of the sonde data. The recent study by *Miloshevich et al.* [2006] discusses uncertainties in water vapor measurements from radiosondes.

2.4 MODIS

The Moderate Resolution Imaging Spectroradiometer (MODIS) is a scanning spectroradiometer with 36 visible, near-infrared, and infrared spectral bands between 0.553 and 14.235 μm (*King et al.*, 1992). There are two MODIS instruments currently in operation: one on Terra, which was launched in December 1999, and one on Aqua, which was launched in May 2002. The operational MODIS algorithm for retrieving atmospheric temperature and moisture distributions, total column ozone burden, and integrated total precipitable water vapor (TPW) from MODIS infrared radiances has been described in detail by *Seemann et al.* [2003]. In particular, water vapor mixing ratio is retrieved at 101 fixed pressure levels from the clear-sky radiances

measured in the 11 MODIS infrared bands between 4.482 and 14.385 μm within a 5 x 5 pixel field of view (approximately 5-km resolution) over land and ocean for both day and night. TPW is then calculated by integrating over the 101 levels. In fact, MODIS does not have high enough spectral resolution to yield independent information at that many vertical levels, so the archived MODIS Level 2 atmospheric profile product (MOD07_L2 for MODIS-Terra, and MYD07_L2 for MODIS-Aqua) includes retrieval results at only 20 atmospheric pressure levels, in addition to TPW. All MODIS water vapor products used in this paper were derived from integration of the 101-level retrievals from the most recent version, V5.2, of the MODIS IR retrieval algorithm. There is a separate MODIS algorithm [*Gao and Kaufman*, 2003] that uses data measured at 1-km resolution in five near-infrared MODIS channels centered between 0.865 and 1.24 μm to derive total precipitable water vapor during daytime over clear land areas, over the extended glint area over clear ocean areas, and above clouds over both land and ocean. These data are not considered in this paper because our measurements focused on cloud-free locations outside the MODIS glint over the Gulf of Maine. Terra and Aqua are sun-synchronous satellites, with Terra's sunlit overpasses occurring in the local morning and Aqua's in the local afternoon. Local equator crossing times for Terra and Aqua are ~10:30 AM and ~1:30 PM, respectively. Both MODIS water vapor products are particularly well-suited for measuring spatial variability in column water vapor due to their high spatial resolution.

2.5 AIRS

The Atmospheric Infrared Sounder (AIRS) experiment actually consists of three separate instruments on the Aqua satellite. AIRS was designed to obtain continuous global measurements of the Earth's atmospheric water vapor and temperature profiles. The AIRS instrument is a

hyperspectral nadir cross-track scanning infrared spectrometer with a 15 km field of view (FOV) [*Pagano et al.*, 2003]. Also on Aqua are two multichannel microwave sounders: the Advanced Microwave Sounding Unit (AMSU-A) with a 45 km FOV and the Humidity Sounder for Brazil (HSB) with a 15 km FOV [*Lambrigtsen*, 2003; *Lambrigtsen and Calheiros*, 2003]. Both AIRS and AMSU-A continue to operate, but the HSB ceased operation in early February 2003 due to a mirror scan motor failure. AIRS geophysical retrievals [*Susskind et al.*, 2003, 2006; *Aumann et al.*, 2003] use the infrared and the microwave measurements. Like AIRS, the AMSU-A is also a cross-track scanner, but it scans three times as slowly as AIRS (once per 8 seconds) and its footprints are approximately three times as large as those of AIRS (45 km at nadir). These differences result in three AIRS scans per AMSU-A scan and nine AIRS footprints per AMSU-A footprint. AIRS data retrievals are generated at the nominal 45-km nadir resolution of the AMSU in granules, which consist of 45 cross-track scans of the AMSU-A mirror. Each scan consists of 30 contiguous AMSU FOVs. The relatively coarse horizontal resolution of the AIRS retrievals prevents comparing them to the fine-scale horizontal structure (e.g., gradients) measured by AATS within a typical J31 transect. However, the AIRS retrievals are unique in providing measurements of the vertical distribution of water vapor at a resolution of 1-2 km in altitude. In this paper, we include only data extracted from the AIRS high vertical resolution (100 pressure levels) Version 4.0 L2 Support Atmospheric/Surface Product files. Additional details on instrument and data acquisition specifications for the AIRS instrument suite can be found in the AIRS/AMSU/HSB Version 4.0 Data Release User Guide [*Olsen et al.*, 2005a; *Aumann et al.*, 2003].

3. Results

3.1 Comparison of AATS water vapor retrievals with coincident J31 Vaisala HPM243 measurements and with near-coincident ship balloonsonde measurements

In this section we compare AATS-14 water vapor retrievals with coincident J31 Vaisala HMP243 measurements acquired during 35 aircraft vertical profiles, and we also compare AATS-14 and J31 Vaisala retrievals with near-coincident measurements acquired by 46 radiosondes (including 4 ozonesondes) launched from the NOAA R/V Ron Brown.

Figure 2 overplots CWV profiles calculated from AATS-14 and J31 Vaisala measurements obtained during 35 separate J31 ascents and descents. Because the J31 Vaisala cannot measure CWV above the J31 altitude, each Vaisala CWV profile has been set equal to the AATS-14 CWV value at the top of the profile. The units of CWV are g/cm^2 or, equivalently, cm – the typical units of precipitable water vapor. The corresponding differences are plotted in Figure 3. In general, the largest differences occur at the lowest altitudes and can be explained by the nature of the measurements. The basic AATS water vapor retrieval is an integrated quantity, whereas the basic J31 Vaisala water vapor retrieval is a height-resolved water vapor density. The AATS-14 retrieval at each altitude represents an instantaneous measurement of the total water vapor in the column above the J31 altitude. On the other hand, the J31 Vaisala CWV value at a particular altitude is calculated by integrating the Vaisala-measured water vapor density profile from that altitude to the top of the J31 profile and then adding the amount of CWV measured by AATS at the top of the profile. Because the J31 took 7 to 24 minutes to complete each profile shown in Figures 2 and 3, each Vaisala CWV value includes data sampled over a range of times and aircraft locations. Hence, the difference between the AATS instantaneous CWV and the Vaisala

time- and space-integrated CWV at a specific altitude includes temporal and/or spatial atmospheric differences (in addition to any differences in measurement technique, calibration, etc.).

Figure 4 overplots Vaisala and AATS-14 water vapor density (ρ_w) profiles for the same J31 profiles shown in Figures 2 and 3. Due to the nature of the remote measurement that includes temporal and spatial atmospheric variability and requires some vertical smoothing, the AATS-14 water vapor density retrieval generally cannot yield the fine vertical resolution provided by the in-situ J31 measurement. Nevertheless, as is evident in Figure 4, the agreement between the in-situ and remotely-measured profiles is quite good. Water vapor horizontal and/or temporal inhomogeneities can lead to AATS measurements of increasing CWV with altitude and result in physically implausible (i.e., negative) retrievals of water vapor density at specific altitudes, as can be seen, for example, in the profiles for 26 July in Figure 4. Additional vertical smoothing would eliminate these negative retrievals, but at a cost of reduced vertical resolution that would essentially discard useful profile information. Hence, there is a tradeoff between vertical resolution and accuracy of the AATS ρ_w profiles. The optimum tradeoff depends in part on the actual vertical structure in water vapor in a given profile.

Figure 5 quantifies the comparison between the AATS-14 and J31 Vaisala water vapor retrievals. Figure 5a is a scatterplot of AATS versus J31 Vaisala water vapor in the layer bounded by the bottom and top of the J31 profile for the 35 profiles shown in Figure 1. The data are highly correlated, with an r^2 correlation coefficient of 0.96, but AATS LWV retrievals are biased 7.1% low relative to the Vaisala values, with an rms difference of 0.21 g/cm^2 (8.9% of the mean J31

Vaisala value). Figure 5b is a corresponding scatterplot of AATS versus Vaisala ρ_w at all altitudes. The correlation is nearly the same as that for CWV shown in Figure 5a, with an r^2 coefficient of 0.95; the rms difference and bias are 20.2% and -7.1%, respectively.

In Figure 6, we compare AATS and J31 Vaisala LWV with Ron Brown sonde LWV obtained by integrating the sounding data over the altitude range defined by the J31 profile. Figures 6a (AATS versus sonde) and 6c (J31 Vaisala versus sonde) show results for all ship soundings (46, including 4 ozonesondes) within 3 hr of the 35 J31 profiles, with no screening by distance from the plane to the sounding. Corresponding r^2 values are 0.56 and 0.58, with rms differences of ~0.42 g/cm^2, or ~18% of the sonde value. Agreement improves markedly if only ship soundings within one hour and 130 km of the J31 profile are included in the comparisons. These results are shown in Figures 6b and 6d, with r^2 values of 0.90 and 0.92, and rms differences of 0.26 g/cm^2 (10.7%) and 0.20 g/cm^2 (8.4%), indicating the importance of collocation or the need for an independent assessment of spatial variability for the interpretation of satellite and suborbital data. AATS LWV values are biased 5.5% less than sonde values, and J31 Vaisala values are 2.3% higher.

3.2 MODIS-AATS water vapor comparisons

Coincident AATS-14 CWV retrievals were obtained over the ocean at aircraft altitudes below 120 m and within one hour of satellite overpass for five MODIS-Terra and five MODIS-Aqua overpasses for which MODIS IR retrievals of water vapor profiles have been derived. There were 203 MODIS IR retrieval grid cells (nominally 5 x 5 1-km pixels per cell at nadir) that contained low-altitude J31/AATS flight segments (for Terra: 124 cells on 17, 20, 22, and 29 July

and 2 August; for Aqua: 79 cells on 12, 16, 21, and 23 July and 8 August). Because the MODIS TPW product is for the full atmospheric column and all AATS measurements were obtained at altitudes above the sea surface, for each MODIS grid cell containing coincident AATS retrievals we have integrated the MODIS 101-level profile of water vapor mixing ratio above the altitude of the J31 for direct comparison to AATS CWV. In practice, this integral was performed over pressure (with linear interpolation between MODIS atmospheric pressure levels, as necessary) for all altitudes above the level corresponding to the mean atmospheric pressure measured on the J31 for all AATS CWV retrievals within the particular MODIS grid cell. In this section, we first illustrate the MODIS-AATS comparisons by analyzing in detail one day, 21 July 2004, and then we summarize all the MODIS-AATS comparisons in terms of scatter plots.

No screening based on the MODIS quality assurance flags has been applied to the MODIS retrievals used in our analysis. All retrievals have been tagged as useful by the MODIS IR quality assurance flag for TPW, but according to the most recent MODIS Atmosphere QA plan [*Hubanks*, 2005], this flag is not reliable in regions designated not useful/bad and results in not useful pixels being incorrectly tagged as useful about 50% of the time. Regarding the MODIS cloud mask, *Seemann et al*. [2003] note that the MODIS retrieval algorithm requires that at least 5 of the 25 pixels in a 5 x 5 field-of-view area have a 95% or greater confidence of clear by the cloud mask and the retrieval uses the average radiance of only those pixels flagged as clear. In this paper, 186 of 203 cells included at least 20 pixels flagged as clear. Only 3 of the remaining 17 cells included fewer than 11 clear pixels, and in none of the 17 cells did the retrieved TPW value differ markedly from the values in the adjacent cells.

Figure 7a presents a map view of the J31 flight track overlain on the MODIS IR (nominally 5x5 km) grid cells for the MODIS-Aqua overpass at 1806 UT on 21 July. The entire J31 track is shown as a thin dashed black line. For those flight segments during the time period 17.9-18.4 UT when the J31 flew at or below 120 m GPS altitude, the amount of CWV measured by AATS along the track is color-coded in increments of 0.05 g/cm^2 (= 0.05 cm). MODIS grid cells are color-coded using the same color scheme for the MODIS retrievals of TPW. There are 27 MODIS grid cells that contain AATS low-altitude retrievals; the number of AATS retrievals within each of these cells is printed at the center of the cell. The J31 descent during the period 17.65-17.93 UT (just before the low altitude segment) is annotated, and the location of the Ron Brown at 42.56°N, 70.56°W is also shown. Figure 7b overplots time (i.e., along track) traces of aircraft altitude and AATS-retrieved CWV for the 17.6-18.4 UT period. AATS CWV retrievals after the J31 descent ranged from 2.4 to 2.85 g/cm^2, but values obtained at altitudes at or below 120 m were ≥2.65 g/cm^2. At the actual time of satellite overpass, the J31 had climbed above 120 m altitude in order to safely execute a turn from a NE heading to a WNW heading. This is also reflected in Figure 7a by the gap in AATS CWV color coding along the flight track at that time.

In Figure 8, we compare MODIS retrievals of TPW and CWV with mean AATS CWV retrievals within each of the 27 MODIS grid cells for the 21 July Aqua overflight. Representative uncertainties are also shown. As noted in Section 2.1, the uncertainty in AATS CWV has been calculated according to *Schmid et al*. [1996]. The MODIS uncertainty has been estimated as 0.05 g/cm^2, as there is no published uncertainty yet. Figure 8a indicates that for this case MODIS and AATS CWV retrievals are poorly correlated ($r^2 = 0.10$), and the comparison suggests that, for the ensemble, MODIS CWV appears to underestimate AATS CWV by about

0.10 g/cm^2 (3.6%), with an rms difference of 0.13 g/cm^2 (4.7%). However, we note that for the majority of data points the departure from the one-to-one correspondence line is within the respective uncertainty estimates. The absolute differences are plotted in Figure 8b.

For this case, we have also compared CWV measurements derived from a radiosonde that was launched from the NOAA R/V Ron Brown at 17 UT with the corresponding AATS and J31 Vaisala data acquired during the J31 17.65-17.93 UT descent that preceded the low altitude transect. The mean distance between the radiosonde and the location of the J31 during its descent was 83.5 km. We do not show these results, but the three sets of CWV profile measurements are in excellent agreement, with J31 Vaisala/AATS and sonde/AATS r^2 values near 1.00 and rms differences of 0.05 g/cm^2 (6% of the mean AATS value) and 0.03 g/cm^2 (4%), respectively. LWV values in the layer traversed by the J31 (5.588 – 0.125 km) during its descent were 2.63, 2.78, and 2.72 g/cm^2 for AATS, J31 Vaisala, and Ron Brown sonde, respectively. Corresponding CWV values measured or derived from measurements obtained by the three sensors at the minimum altitude of the J31 profile were 2.69, 2.84, and 2.79 g/cm^2, respectively. The amount of water vapor measured by the sonde in the layer between the lowest altitude (0.011 km) sampled by the sonde and the bottom of the J31 profile at 0.125 km was 0.174 g/cm^2, which yields a vertical water vapor gradient of ~-0.15 g/cm^2 per 100 m. One could use this vertical gradient to increase each of the AATS CWV measurements by the amount of water vapor below the aircraft for direct comparison with MODIS TPW. This would result in increases from 2% to 6% of the retrieved AATS CWV values. Although we have opted in favor of the more direct approach of integrating each of the 27 MODIS profiles to calculate MODIS CWV above the mean pressure (altitude) of the J31 (and, in fact, temporally and spatially near-

coincident radiosonde measurements were not available for most J31/satellite comparisons), it is interesting to note that the sonde vertical water vapor gradient (-0.15 g/cm^2 per 100 m) below the J31 exceeded the corresponding mean vertical gradient (-0.09 ± 0.02 g/cm^2 per 100 m) obtained from the MODIS profiles by ~70%.

Figure 9 presents scatterplots of MODIS CWV and MODIS minus AATS CWV versus AATS CWV for all 203 grid cells containing AATS retrievals during the 10 satellite overpasses. The correlation is poor (r^2 = 0.20), and bias and rms differences are rather large: 0.55 g/cm^2 (21%) and 0.27 g/cm^2 (10%), respectively. However, this may be misleading, because the statistics improve dramatically if retrievals from 12 July (Aqua), 22 July (Terra), and 2 August (Terra) are omitted, because MODIS CWV retrievals significantly overestimate (by ~15-70%) the AATS values in all cells for those overpasses. Omitting these cases yields an r^2 of 0.85, an rms difference of 0.20 g/cm^2 (7.8%), and a bias of -0.03 g/cm^2 (-1.3%). We have no explanation for this behavior at this time, but we are continuing to investigate it.

In Figure 10, we stratify the data by satellite, with MODIS-Aqua results shown in Figure 10a and MODIS-Terra results presented in Figure 10b. In light of the discussion above, the results are not surprising. MODIS-Aqua retrievals agree with AATS CWV retrievals better than MODIS-Terra retrievals. MODIS-Aqua retrievals are biased high (0.31 g/cm^2, or 13.7%), with an rms difference of 0.12 g/cm^2 (5.1%). If the 12 July case is omitted, these values decrease to 0.19 g/cm^2 (8.2%) and 0.07 g/cm^2 (3.0%), respectively, with r^2 increasing from 0.51 to 0.86. Because of the large differences on 22 July and 2 August, the MODIS-Terra retrievals are essentially uncorrelated with the AATS values (r^2=0.05), and the comparisons yield an rms difference of

0.65 g/cm^2 (24.1%) and a bias of 0.36 g/cm^2 (13.4%). As expected, omitting results from 22 July and 2 August significantly improves the agreement, with an r^2 of 0.74, an rms difference of 0.22 g/cm^2 (7.4%), and a bias of -0.17 g/cm^2 (-5.7%).

3.3 AIRS-AATS water vapor comparisons

The high spectral resolution of AIRS yields retrievals that contain much more information on the vertical distribution of water vapor than is possible from MODIS measurements, which have the horizontal resolution to better identify horizontal variability in total columnar water vapor. During ITCT, J31 ascents and/or descents near the time of the Aqua satellite overpass afforded the unique opportunity to compare coincident airborne remote (AATS-14) and in-situ (Vaisala HMP243) measurements with AIRS over-ocean water vapor profile retrievals. Previously, *Gettelman et al.* [2004] presented results from comparisons of AIRS oceanic water vapor retrievals and aircraft in-situ water vapor measurements acquired in the upper troposphere and lower stratosphere. Other studies that have addressed or at least included validation of AIRS over-ocean water vapor retrievals have included only radiosonde measurements [*Tobin et al.*, 2006; *Fetzer et al.*, 2003], or a combination of sonde, other satellite sensor measurements, and/or numerical model results [*Fetzer et al.*, 2006; *Divakarla et al.*, 2006]. To our knowledge, ours is the first study that uses temporally and spatially coincident or near-coincident aircraft in-situ and remote sensor measurements to validate AIRS over-ocean water vapor retrievals in the lower troposphere. We have identified eight Aqua overpasses for which AATS water vapor retrievals are available during near-coincident J31 vertical profiles. There were 14 separate J31 profiles flown within 90 minutes of these eight Aqua overpasses, including 11 within one hour of the overpass time. In particular, these were: 1 profile each on 12, 15 and 31 July, and on 8 August; 2

profiles each on 23 and 29 July; and 3 profiles each on 16 and 21 July. In this section, we compare AIRS retrievals with AATS and J31 Vaisala water vapor retrievals derived from measurements obtained during these 14 aircraft profiles.

As noted in Section 2.5, we use only AIRS data extracted from the AIRS high vertical resolution (100 pressure levels) Version 4.0 L2 Support Atmospheric/Surface Product files. Although the 100-level profiles actually over-resolve the vertical structure, they are particularly useful for calculating integral quantities (as done here) or in radiative transfer calculations (for which they were designed). Specifically, these files include the retrieved layer water vapor (molecules/cm^2) within the layers bounded by adjacent pressure levels. These values are stored in a three-dimensional variable (100,30,45), where the first dimension specifies the pressure level, the second specifies sub-satellite location along the satellite track, and the third specifies the across-track location. AIRS retrievals are available at 31 pressure levels (each corresponding to the base of a layer) between 407.47 mb (~maximum altitude attained during any J31 profile) and 1100 mb. For each profile, the index of the first pressure level above the mean surface is also included in the archived data files and, because the retrievals below this surface are extrapolated, the surface value must be calculated by interpolation [*Olsen et al.*, 2005b]. The AIRS retrieval data sets include numerous control flags that provide information about the quality of the retrieved products. These are discussed in detail in *Susskind et al.* [2006]. Following *Tobin et al.* [2006] and *Fetzer et al.* [2006], we screen the AIRS retrievals by using two of the AIRS quality flags: *Qual_H2O* and *Qual_Temp_Profile_Bot*. These can have values of 0, 1, or 2 corresponding to retrievals of highest, good, and poor (unacceptable) quality, respectively. *Qual_H2O* is the overall quality flag for water vapor and equals zero if the microwave-only part

of the retrieval algorithm converged. *Qual_Temp_Profile_Bot* indicates temperature convergence in the lowest 3 km of the profile, but it equals zero only if the IR temperature profile retrieval algorithm converged throughout the profile. As noted by *Fetzer et al.* [2006], since the temperature solution from the IR observations must converge for the water vapor solutions to proceed, retrievals with *Qual_Temp_Profile_Bot* = 0 have the highest information content.

3.3.1 21 July Aqua Overpass

We compare AIRS water vapor retrievals with J31 AATS and Vaisala water vapor measurements by examining differences for (1) the layer defined by the bottom and top of J31 profiles, and (2) the individual layers defined by the AIRS retrieval pressure levels. To set the stage for these comparisons, we first show retrievals for one case – the 21 July Aqua overpass at 1806 UT and the coincident J31 spiral descent from 5.588 km to 0.125 km during the period 17.6-17.9 UT. Figure 11a presents a map view of the J31 flight track (color-coded by aircraft altitude) on 21 July and the center point locations of the 20 AIRS profile retrievals within 150 km of the J31 profile. The J31 flight pattern on this day also included a ramped ascent (17.1-17.4 UT) after takeoff from Pease, and another spiral descent from 18.9 to 19.1 UT. Figure 11b overplots the CWV profiles measured by AATS and by the J31 Vaisala during the J31 descent with the AIRS CWV profile retrieved within each of the AMSU footprints centered at the locations shown in Figure 11a. (Recall that although each AMSU footprint encompasses nine AIRS footprints, only one AIRS water vapor retrieval at the coarser AMSU resolution is archived for each AMSU footprint.) The AIRS retrievals use the same symbol and color scheme shown in Figure 11a, and the legend also includes the across-track (first – e.g., 25) index and

along-track (second – e.g., 9) index corresponding to the indices listed next to each AIRS center location shown in Figure 11a. The vertical coordinate in Figure 11b and in subsequent plots showing AIRS data is atmospheric pressure, because that is the vertical coordinate included in the AIRS product files and it is routinely measured on the J31. The AIRS CWV at each altitude has been calculated by summing all AIRS layer water vapor values at and above that altitude. The AIRS data points at the largest pressure (lowest altitude) for each retrieval have been calculated using the interpolation procedure prescribed by *Olsen et al.* [2005b].

For comparison with the archived AIRS water vapor retrievals within specified pressure layers, we have interpolated within the AATS and J31 Vaisala water vapor retrievals to calculate the amount of water vapor, LWV_A, within the layers defined by the AIRS pressure levels for which J31 data are available. Here we use the acronym LWV_A to distinguish from LWV, the water vapor in the layer bounded by the minimum and maximum altitudes of the J31 profile. In Figure 12, we overplot AIRS LWV_A retrievals centered at each of the 20 locations shown in Figure 11a with the AATS and J31 Vaisala LWV_A calculated from the measurements acquired during the 17.6-17.9 UT J31 descent. The frames shown in this figure are arranged from left to right and top to bottom to correspond to the AIRS retrievals across (longitudinal ~W to E) and along (latitudinal ~S to N) the satellite track. Each frame is labeled with the across track and along track index of the AIRS center point location, and also includes the distance (km) from that point to the mean location of the J31 profile. A number of the AIRS retrieved profiles (c.f., profiles at locations [25,10], [26,10], [26,11]) appear to agree quite well with the AATS and Vaisala retrievals. In order to investigate this quantitatively, we have applied this analysis approach to

all ITCT J31/AIRS near-coincident profile measurements. These results will be discussed in detail and shown in Figures 18-21 below.

3.3.2 Layer Water Vapor (LWV) comparisons for J31 profile layers

We have calculated LWV for AIRS profile retrievals within 150 km of each J31 profile by integrating the AIRS data. For each profile, the corresponding value of LWV for AATS has been calculated for each profile by subtracting the CWV measured at the top of the profile from that measured at the bottom, and for the J31 Vaisala by integrating its ρ_w measurements. In Figure 13, we explore the behavior of the absolute and relative AIRS minus AATS LWV differences as a function of the distance from the AIRS retrieval center point location to the mean location of the J31 profile. In this figure, all AIRS retrievals within 150 km of the J31 for a particular J31 profile have been color-coded using the same symbol/color combination, but a different combination has been used to identify data pertaining to each J31 profile. Figure 13a shows the absolute LWV differences, and Figure 13b shows the relative differences. For each profile, the legend lists the date, Aqua overpass time, J31 profile times, and vertical extent (in mb) of each J31 profile. Most mean LWV differences fall between -0.6 g/cm^2 (~20% of the AATS value) and +1.0 g/cm^2 (~50% of the AATS value) for AIRS profiles within 100 km of the J31 profile.

Figure 14 is a scatterplot of AATS versus J31 Vaisala LWV for the 14 aircraft profiles. As expected, the correlation is high, with an r^2 of 0.987; and the agreement is very good, with values of 1.000 and -0.098 for the slope and intercept, respectively, of the regression line. The AATS retrievals underestimate the J31 Vaisala LWV retrievals by ~0.10 g/cm^2 (4.3%), with an rms

difference of 0.13 g/cm^2 (5.5%). Figures 15 and 16 present scatterplots of AIRS versus AATS and AIRS versus J31 Vaisala LWV, respectively. Only those AIRS retrievals for which *Qual_H2O* = 0 have been included in the analyses. Figures 15a,b present results for AIRS retrievals within 150 km of a particular J31 profile for *Qual_Temp_Profile_Bot* = 2 and *Qual_Temp_Profile_Bot* = 0, respectively. Figures 15c,d show analagous results for AIRS retrievals within 80 km. Figure 16 presents analogous plots for AIRS/J31 Vaisala comparisons. Examination of these figures and Table 2, which lists the statistics of the comparisons, leads to the following observations:

- AIRS LWV retrievals generally exceed AATS-14 and J31 Vaisala measurements. AIRS retrievals agree somewhat better with the Vaisala than with the AATS-14 values, and this is consistent with the finding that AATS measurements are biased 4.3% low relative to the Vaisala measurements.

- The number of AIRS retrievals included in the analyses decreases significantly if AIRS data are screened by distance and/or by the *Qual_Temp_Profile_Bot* quality flag. The number of retrievals ranges from a maximum of 305 for *Qual_Temp_Profile_Bot* = 2 and a maximum distance threshold of 150 km to a minimum of 36 for *Qual_Temp_Profile_Bot* = 0 and a distance threshold of 80 km.

- For the AIRS-AATS and the AIRS-Vaisala comparisons, agreement improves if AIRS retrievals are limited to those located within 80 km of the J31 profile. For AIRS-AATS, rms differences decrease from 21.5% (150 km) to 16.4% (80 km) for the highest information content AIRS water vapor retrievals (*Qual_Temp_Profile_Bot* = 0). The analogous decrease

for AIRS-Vaisala is 18.5% to 12.8%. Corresponding bias differences decrease from 8.8% to 5.8% for AIRS-AATS and from 4.0% to 1.0% for AIRS-Vaisala.

- For each AIRS-J31 sensor comparison, for a distance threshold of 150 km the r^2 values and rms differences improve slightly and the bias differences show little change after more stringent screening is applied by use of the *Qual_Temp_Profile_Bot* flag. For a distance threshold of 80 km, the r^2 values and rms differences show little dependence on *Qual_Temp_Profile_Bot*, but bias differences decrease with more stringent screening.

The rationale for discriminating by the distance from the AIRS profile to the J31 profile and for limiting the scatter plots to all profiles within 150 km and to those within 80 km is shown in Figure 17. This figure examines the variation of r^2 for AIRS-AATS and for AIRS-Vaisala comparisons as a function of the maximum allowable distance; it includes values of r^2 that have been calculated at 10-km increments in distance. Figure17a presents results for *Qual_Temp_Profile_Bot* = 2 and shows that r^2 decreases markedly for distance thresholds between 30 and 50 km and even more dramatically beyond 80 km. For retrievals with *Qual_Temp_Profile_Bot* = 0 (Figure 17b), the largest decreases in r^2 occur between 50 and 70 km, and beyond 110 km. Nevertheless, if the results for distances less than 50 km are ignored due to the relatively low number of AIRS retrievals at those distances, then a maximum distance threshold of 80 km appears to be a reasonable choice for presentation of the results.

3.3.3 Layer Water Vapor (LWV_A) comparisons for AIRS pressure layers

In Figures 18-21, we compare AIRS retrievals of layer water vapor, LWV_A, for 26 layers defined by the AIRS pressure levels between 986.07 mb and 407.5 mb with corresponding J31 retrievals

of LWV_A calculated for the same layers. The AATS and Vaisala values were calculated by interpolation within the AATS and Vaisala measurements, as described above. Results are presented for AIRS LWV_A retrievals for *Qual_Temp_Profile_Bot* values of 0 and 2 for maximum distance thresholds of 150 km and 80 km, each. Figure 18a overplots the results for AIRS and AATS for *Qual_Temp_Profile_Bot* = 2 and a distance threshold of 150 km. The mean and range of LWV_A in each pressure layer are plotted at the bottom pressure boundary. The number of AIRS retrievals included in each pressure layer and the number of J31 sensor observations are also shown. Figure 18b shows mean (bias) and rms AIRS minus AATS LWV_A differences, and Figure 18c presents the relative differences. Mean and rms percent differences have been weighted by the amount of water vapor in the layer, in keeping with the approach used by Susskind et al. [2003] and Tobin et al. [2006]. Corresponding results for the AIRS-Vaisala comparison are presented in Figures 18d-f. Figure 19 presents analogous results for *Qual_Temp_Profile_Bot* = 0 and a distance threshold of 150 km; Figures 20 and 21 show the results for a distance threshold of 80 km.

Examination of Figures 18-21 leads to the following observations regarding comparisons of LWV_A:

- As expected, all three sensors yield retrievals that decrease with altitude. The AATS retrievals appear to show more structure than do the retrievals from the in-situ and the satellite sensors. This result is attributed to the nature of the basic AATS measurement, CWV, that is dependent on the total amount of water vapor in the column above the sensor at each altitude and hence more sensitive to horizontal inhomogeneities in total CWV than the other two

sensors. However, both J31 sensors are susceptible to water vapor spatio-temporal variability due to advection or spatial inhomogeneity during the aircraft profile.

- When all AIRS profiles within 150 km of the J31 profiles are included, AIRS retrievals exhibit positive excursions from the mean that are 2-4 times the corresponding AATS and Vaisala values, as evidenced by the respective range of observed retrievals (purposely truncated in Figures 18a,d and 19a,d, but AIRS negative excursions are less than those of AATS or the Vaisala.

- When AIRS profile retrievals within 150 km of the J31 and with *Qual_Temp_Profile_Bot* = 2 are included, AIRS mean retrievals exceed corresponding AATS means in all layers below 600 mb, with biases ranging from ~0.005 to 0.025 g/cm^2. Since these AIRS profiles are the lowest quality AIRS retrievals, they were not expected to agree well with the AATS data. Nevertheless, relative biases are generally <10% for layers below 707 mb (top of the layer with the base at 730 mb). Relative biases are generally 20-30% between 700 and 600 mb. The one exception is the large bias of ~0.025 g/cm^2 (~55%) for the 684-661 mb layer. This is attributed to spatial or temporal variability in the water vapor during one or more J31 profiles included in the mean and leads to slightly negative AATS LWV_A retrievals near 700 mb in those few profiles and an artificially low mean value in the layer between 707 and 684 mb. This behavior is also reflected in the J31 Vaisala retrieval in this layer, but to a lesser degree. The peak in the AIRS-AATS bias in the layer with its base at 958 mb is likely also due to atmospheric variability in the CWV above the J31 that results in an artificially low mean AATS retrieval. This is absent in the AIRS-Vaisala comparison. In fact, if the points at 958 mb and 730 mb in the AIRS-AATS bias curve were omitted, then the AIRS-AATS and AIRS-

Vaisala bias curves would have essentially the same shape. The absolute and relative bias and rms differences are slightly less for the AIRS-Vaisala comparisons than for the AIRS-AATS comparisons. Both sets of comparisons exhibit large relative rms differences above 700 mb due to the small mean LWV_A values at those altitudes. For *Qual_Temp_Profile_Bot* = 0 (Figure 19), results change only slightly. The number of AIRS retrievals included in the analysis for each layer decreases significantly (by up to 70% for the 754-730 mb layer), but the largest change in the statistics is a small increase in the biases and rms differences for layers below 800 mb.

- As expected, restricting the analysis to AIRS profiles located within 80 km of the J31 (Figures 20 and 21) also reduces the number of AIRS retrievals in each layer (at least below 500 mb) significantly from the number included for a distance threshold of 150 km. For AIRS LWV_A retrievals, resultant positive excursions from the mean decrease markedly, and the range of values becomes comparable to the range of the AATS and Vaisala retrievals. Bias and rms difference curves shift to the left (or smaller values for rms differences and positive bias), with an increase in the number of negative bias values, especially below 750 mb. Mean AIRS-AATS biases are 0-10% below 729 mb, with corresponding rms differences of ~20% below 700 mb and 40-100% above 700 mb. Corresponding AIRS-Vaisala biases are similar, with smaller rms differences above 700 mb.

4. Summary and conclusions

Airborne sunphotometer measurements acquired over the Gulf of Maine during INTEX-ITCT 2004 have been analyzed to yield retrievals of columnar water vapor and profiles of water vapor density. AATS-14 measurements acquired during low level (typically 60-120 m ASL) J31

transects designed to coincide temporally and spatially with satellite overpasses allowed comparison of AATS CWV with MODIS over-ocean IR retrievals of CWV obtained during 5 Aqua and 5 Terra overpasses. AATS water vapor profile retrievals have been compared with simultaneous in-situ measurement of water vapor density by an onboard Vaisala humidity sensor and with temporally and spatially near-coincident measurements by radiosondes released from the NOAA R/V Ronald H. Brown. AATS and J31 Vaisala profile measurements obtained near the time of satellite overpass have also been compared with AIRS water vapor retrievals from data obtained during 8 Aqua overpasses.

Comparison of AATS-14 and J31 Vaisala retrievals of the amount of LWV during 35 aircraft vertical profiles gave an r^2 of 0.96 and an rms difference of 0.21 g/cm^2 (8.9%). Comparison of corresponding ρ_w values calculated at 20-50 m vertical resolution for all of these profiles gave an r^2 of 0.95 and an rms difference of 0.91 g/m^3 (20.4%). For the composite data sets, AATS retrievals of LWV and ρ_w slightly underestimated the corresponding Vaisala retrievals by amounts that increased with increasing LWV and ρ_w, with biases of about -7%. In comparing AATS-14 water vapor measurements with simultaneous measurements obtained by a Vaisala HMP243 and an EdgeTech 137-C3 chilled mirror aboard the Twin Otter during ACE-Asia (Aerosol Characterization Experiment-Asia), *Schmid et al.* [2003] also measured an AATS dry bias of 7% in ρ_w. In a more recent airborne study (at the ARM-SGP site) using AATS-14 and the EdgeTech chilled mirror aboard the Twin Otter, *Schmid et al.* [2006] report an AATS dry bias of 5% relative to the chilled mirror. This study used a different brand 941-nm filter from that used during ACE-Asia in AATS, and this was the same filter used during INTEX-ITCT 2004. For 22 Ron Brown radiosonde profiles launched within 1 hour and 130 km of a J31

profile, comparisons of AATS and sonde LWV amounts gave an r^2 of 0.90 and an rms difference of 0.26 g/cm^2 (10.7%). Comparison of the corresponding J31 Vaisala and sonde values yielded an r^2 of 0.92 and an rms difference of 0.20 g/cm^2 (8.4%). In the mean, AATS LWV retrievals were 5.5% less than sonde values, and J31 Vaisala values were biased 2.3% greater than sonde values.

AATS measurements obtained during low altitude horizontal transects within one hour of satellite overpass yielded CWV retrievals in 203 MODIS IR retrieval grid cells (5 x 5-km resolution at nadir) during 5 Aqua and 5 Terra overpasses. When retrievals from all 10 overpasses are included in the comparison, the correlation is poor (r^2 = 0.20), and bias and rms differences are 0.55 g/cm^2 (21%) and 0.27 g/cm^2 (10%), respectively. However, MODIS CWV retrievals significantly overestimate (by ~15-70%) the AATS values in all cells (69) for 3 of the 10 overpasses. Omitting these cases significantly improves the agreement, with an r^2 of 0.85, an rms difference of 0.20 g/cm^2 (7.8%), and a bias of -0.03 g/cm^2 (-1.3%). The disagreement observed in these three cases is still being investigated.

The J31 flew 14 profiles within ~1.5 hr of 8 Aqua overpasses for which AIRS water vapor amounts have been retrieved. AATS-14 and J31 Vaisala LWV retrievals were highly correlated (r^2 = 1.00) for measurements acquired during those profiles. However, AATS values underestimated the Vaisala values by 4.3% (bias). We compared these data with the corresponding AIRS water vapor retrievals, which were screened based on AIRS quality control flags and on the distance from the AIRS retrieval to the J31 profile location. We presented results for AIRS retrievals within 150 km and within 80 km of a J31 profile. The number of

AIRS profiles included in the analyses ranged from 305 for the least stringent screening to 36 for the most stringent screening, which was for retrievals with the highest information content within 80 km of the J31 profiles. AIRS retrievals agreed better with J31 sensor measurements when comparisons were restricted to AIRS profiles within 80 km instead of 150 km. In particular, for *Qual_Temp_Profile_Bot* = 0, AIRS-AATS rms differences decreased from 21.5% (150 km) to 16.4% (80 km), and AIRS-J31 Vaisala rms differences decreased from 18.5% to 12.8%. Corresponding bias differences decreased from 8.8% to 5.8%, and from 4.0% to 1.0%, respectively.

We also compared AIRS water vapor retrievals (LWV_A) within the pre-defined AIRS retrieval pressure layers with corresponding AATS and J31 Vaisala retrievals calculated within those layers. In particular, this consisted of 26 layers between 986 and 407 mb. At altitudes below ~900 mb, the maximum AIRS LWV_A retrievals were 2-4 times the corresponding AATS and Vaisala maxima when AIRS observations within 150 km of the J31 profile altitudes were included. However, when the analysis was restricted to AIRS retrievals located within 80 km of the J31, the AIRS LWV_A maxima decreased significantly to values comparable to the J31 sensor retrievals. Relative bias differences varied with altitude but were generally <10% below ~700 mb, ~20-30% between 700 and 600 mb, and more variable above 600 mb. Relative rms differences were ~20% below 700 mb and ≥40% above that altitude.

Acknowledgements

This research is a contribution to the International Consortium for Atmospheric Research on Transport and Transformation (ICARTT), which includes Phase A of the Intercontinental Chemical Transport Experiment (INTEX-A) of the National Aeronautics and Space

Administration (NASA) and the Intercontinental Transport and Chemical Transformation (ITCT) experiment of the National Oceanic and Atmospheric Administration (NOAA). The AATS-14 measurements were supported by NOAA's Atmospheric Composition and Climate Program and by NASA's Programs in Radiation Science, Suborbital Science, and Tropospheric Chemistry. The analyses were supported by NASA's Earth Observing System Inter-Disciplinary Science (EOS-IDS) Program. We thank Dr. Anne Thompson for providing data from ozonesondes launched from the NOAA R/V Ron Brown during the study.

References

Aumann, H. H., et al. (2003), AIRS/AMSU/HSB on the Aqua mission: Design, science objectives, data products, and processing system, *IEEE Trans. Geosci. Remote Sens*., 41, 253-264.

Beer, R. (2006), TES on the Aura Mission: Scientific objectives, measurements, and analysis overview, *IEEE Trans. Geosci. Remote Sens*., 44, 1102-1105.

Bögel, W. (1977), Neue Näherungsgleichungen für den Sättigungsdruck des Wasserdampfes und für die in der Meteorologie gebräuchlichen Luftfeuchte-Parameter, DLR-FB 77-52, Dtsch. Forsch.-und Versuchsanst. Für Luft-und Raumfahrt, Oberpfaffenhofen, Germany.

Bruegge, C. J., J. E. Conel, R. O. Green, J. S. Margolis, R. G. Holm, and G. Toon (1992), Water vapor column abundance retrievals during FIFE, *J. Geophys. Res*., *97*, 18,759-18,768.

Bucholtz, A. (1995), Rayleigh-scattering calculations for the terrestrial atmosphere, *Appl. Opt., 34*, 2765-2773.

Clough, S.A., M.W. Shephard, E.J. Mlawer, J.S. Delamere, M.J. Iacono, K. Cady-Pereira, S. Boukabara, and P.D. Brown (2005), Atmospheric radiative transfer modeling: a summary of the AER codes, *Journal of Quantitive Spectroscopy and Radiative Transfer, 91*, 233-244.

Diner, D. J., et al. (1998), Multiangle Imaging Spectroradiometer (MISR) description and experiment overview, *IEEE Trans. Geosci. Remote Sens., 36*, 1072-1087.

Divakarla, M. G., C. D. Barnet, M. D. Goldberg, L. M. McMillin, E. Maddy, W. Wolf, L. Zhou, and X. Liu (2006), Validation of Atmospheric Infrared Sounder temperature and water vapor retrievals with matched radiosonde measurements and forecasts, *J. Geophys. Res*., *111,* D09S15, doi:10.1029/2005JD006116.

Fehsenfeld, F. C., et al., International Consortium for Atmospheric Research on Transport and Transformation (ICARTT): North America to Europe: Overview of the 2004 summer field study, *J. Geophys. Res*., ICARTT special section, submitted 2006.

Fetzer, E. J., et al. (2003), Validation of AIRS/AMSU/HSB core products for data release version 3.0, August 13, 2003, *JPL D-26538*, 79 pp., NASA Goddard Space Flight Cent., Greenbelt, Md. (Available at http://disc.gsfc.nasa.gov/AIRS/index.shtml/).

Fetzer, E. J., B. H. Lambrigtsen, A. Eldering, H. H. Aumann, and M. T. Chahine (2006), Biases in total precipitable water vapor climatologies from Atmospheric Infrared Sounder and Advanced Microwave Scanning Radiometer, *J. Geophys. Res*., *111,* D09S16, doi:10.1029/2005JD006598.

Gao, B. C., and Y. J. Kaufman (2003), Water vapor retrievals using Moderate Resolution Imaging Spectroradiometer (MODIS) near-infrared channels. *J. Geophys. Res*., *108,* D13, 4389, doi:10.1029/2002JD003023.

Gettelman, A., E. M. Weinstock, E. J. Fetzer, F. W. Irion, A. Eldering, E. C. Richard, K. H. Rosenlof, T. L. Thompson, J. V. Pittman, C. R. Webster and R. L. Herman (2004), Validation of satellite data in the upper troposphere and lower stratosphere with in-situ aircraft instruments, *Geophys. Res. Lett.*, *31*, L22107, doi:10.1029/2004GL020730.

Holben, B. N., T. F. Eck, I. Slutsker, D. Tanré, J. P. Buis, A. Setzer, E. Vermote, J. A. Reagan, Y. J. Kaufman, T. Nakajima, F. Lavenu, I. Jankowiak and A. Smirnov (1998), AERONET—A federated instrument network and data archive for aerosol characterization, *Rem. Sens. Environ*., *66*, 1-16.

Hubanks, P. (2005), MODIS Atmosphere QA Plan for Collection 005, Version 3.0, June 2005 (Available at http://modis-atmos.gsfc.nasa.gov/reference_atbd.html).

Ingold, T., B. Schmid, C. Matzler, P. Demoulin, and N. Kampfer (2000), Modeled and empirical approaches for retrieving columnar water vapor from solar transmittance measurements in the 0.72, 0.82, and 0.94 mm absorption bands, *J. Geophys. Res*., *105,* D19, 24,327, 2000JD900392.

Kaufman, Y. J., D. Tanré, L. A. Remer, E. Vermote, A. Chu, and B. N. Holben (1997), Operational remote sensing of tropospheric aerosol over land from EOS moderate resolution imaging spectroradiometer, *J. Geophys. Res., 102*, 17,051-17,067.

King, M. D., Y. J. Kaufman, W. P. Menzel, and D. Tanre (1992), Remote sensing of cloud, aerosol, and water vapor properties from the Moderate Resolution Imaging Spectrometer (MODIS), *IEEE Trans. Geosci. Remote Sens*., *30*, 2-27.

Lambrigtsen, B. H. (2003), Calibration of the AIRS microwave instruments, *IEEE Trans. Geosci. Remote Sens*., 41, 369-378.

Lambrigtsen, B. H., and R. V. Calheiros (2003), The humidity sounder for Brazil – An international parnership, *IEEE Trans. Geosci. Remote Sens*., 41, 352-361.

Martonchik, J.V., D.J. Diner, R. Kahn, M.M. Verstraete, B. Pinty, H.R. Gordon, and T.P. Ackerman (1998), Techniques for the retrieval of aerosol properties over land and ocean using multiangle imaging, *IEEE Trans. Geosci. Remote Sens., 36*, 1212-1227.

Michalsky, J. J., J. C. Liljegren, and L. C. Harrison (1995), A comparison of sun photometer derivations of total column water vapor and ozone to standard measures of same at the Southern Great Plains Atmospheric Radiation Measurement site, *J. Geophys. Res*., *100*, 25,995-26,003.

Miloshevich, L., H. Vomel, D. Whiteman, B. Lesht, F. Schmidlin, and F. Russo (2006), Absolute accuracy of water vapor measurement from six operational radiosonde types launched during AWEX-G and implications for AIRS validation, *J. Geophys. Res. 111*(D09S10), doi:10.1029/2005JD006083.

Olsen, E. T., editor, et al. (2005a), AIRS/AMSU/HSB Version 4.0 Data Release User Guide, Jet Propulsion Laboratory, California Institute of Technology.

Olsen, E. T., editor, and E. Fishbein, S-Y. Lee, and E. Manning (2005b), AIRS/AMSU/HSB Version 4.0 Level 2 Product Levels and Layers, Jet Propulsion Laboratory, California Institute of Technology.

Pagano, T. S., H. H. Aumann, D. E. Hagan, and K. Overoye (2003), Pre-launch and in-flight radiometric calibration of the Atmospheric Infrared Sounder (AIRS), *IEEE Trans. Geosci. Remote Sens*., 41, 265-273.

Pilewskie, P., O. Hofmann, B. Kindel, W. Gore, P. Russell, J. Livingston, J. Redemann, R. Bergstrom, S. Platnick, J. Daniel, T. Garrett, Cloud Properties Derived from Visible and Near-infrared Reflectance in the Presence of Aerosols, ICARTT JGR, in preparation, 2006.

Reagan, J., K. Thome, B. Herman, R. Stone, J. Deluisi, and J. Snider (1995), A comparison of columnar water-vapor retrievals obtained with near-IR solar radiometer and microwave radiometer measurements, *J. Appl. Meteorol*., *34*, 1384-1391.

Redemann, J., S. Masonis, B. Schmid, T. Anderson, P. Russell, J. Livingston, O. Dubovik, A. Clarke (2003), Clear-column closure studies of aerosols and water vapor aboard the NCAR C-130 in ACE-Asia, 2001, *J. Geophys. Res. 108*(D23), 8655, doi:10.1029/2003JD003442.

Redemann, J., P. Pilewskie, P. Russell, J. Livingston, S. Howard, B. Schmid, J. Pommier, W. Gore, J. Eilers, and M. Wendisch (2006), Airborne measurements of spectral direct aerosol radiative forcing in INTEX/ITCT, *J. Geophys. Res*., accepted February 2006a.

Russell, P. B., J. M. Livingston, E. G. Dutton, R. F. Pueschel, J. A. Reagan, T. E. DeFoor, M. A. Box, D. Allen, P. Pilewskie, B. M. Herman, S. A. Kinne, and D. J. Hofmann (1993a), Pinatubo and pre-Pinatubo optical-depth spectra: Mauna Loa measurements, comparisons, inferred particle size distributions, radiative effects, and relationship to lidar data, *J. Geophys. Res*., *98*, 22,969-22,985.

Russell, P. B., J. M. Livingston, R. F. Pueschel, J. A. Reagan, E. V. Browell, G. C. Toon, P. A. Newman, M. R. Schoeberl, L. R. Lait, L. Pfister, Q. Gao, and B. M. Herman (1993b), Post-Pinatubo optical depth spectra vs. latitude and vortex structure: Airborne tracking sunphotometer measurements in AASE II, *Geophys. Res. Lett*., *20*, 2571-2574.

Russell, P. B., J. M. Livingston, R. F. Pueschel, J. J. Bauman, J. B. Pollack, S. L. Brooks, P. Hamill, L. W. Thomason, L. L. Stowe, T. Deshler, E. G. Dutton, and R. W. Bergstrom (1996), Global to microscale evolution of the Pinatubo volcanic aerosol derived from diverse measurements and analyses, *J. Geophys. Res*., *101*, 18,745-18,763.

Russell, P. B., J. M. Livingston, J. Redemann, B. Schmid, S. A. Ramirez, J. Eilers, R. Kahn, A. Chu, L. Remer, P. K. Quinn, M. J. Rood, and W. Wang, Multi-grid-cell validation of satellite aerosol property retrievals in INTEX/ITCT/ICARTT 2004 (2006), *J. Geophys. Res*., ICARTT special section, submitted.

Schmid, B., and C. Wehrli (1995), Comparison of sun photometer calibration by Langley technique and standard lamp*, Appl. Opt*., *34*, 4500-4512.

Schmid, B., K. J. Thome, P. Demoulin, R. Peter, C. Matzler, and J. Sekler (1996), Comparison of modeled and empirical approaches for retrieving columnar water vapor from solar transmittance measurements in the 0.94-μm region, *J. Geophys. Res*., *101*, 9345-9358.

Schmid, B., P. R. Spyak, S. F. Biggar, C. Wehrli, J. Sekler, T. Ingold, C. Mätzler, and N. Kämpfer (1998), Evaluation of the applicability of solar and lamp radiometric calibrations of a precision Sun photometer operating between 300 and 1025 nm, *Appl. Opt., 37*, 3923-3941.

Schmid, B., Livingston, J. M., Russell, P. B., Durkee, P. A., Collins, D. R., Flagan, R. C., Seinfeld, J. H., Gasso, S., Hegg, D. A., Ostrom, E., Noone, K. J., Welton, E. J., Voss, K., Gordon, H. R., Formenti, P., and M. O. Andreae (2000), Clear sky closure studies of lower tropospheric aerosol and water vapor during ACE 2 using airborne sunphotometer, airborne in-situ, space-borne, and ground-based measurements. *Tellus B 52*, 568-593.

Schmid, B., J. J. Michalsky, D. W. Slater, J. C. Barnard, R. N. Hathore, J. C. Liljegren, B. N. Holben, T. F. Eck, J. M. Livingston, P. B. Russell, T. Ingold, and I. Slutsker (2001), Comparison of columnar water-vapor measurements from solar transmittance methods, *Appl. Opt.*, *40*, 1886-1896.

Schmid, B., J. Redemann, P. B. Russell, P. V. Hobbs, D. L. Hlavka, M. J. McGill, B. N. Holben, E. J. Welton, J. R. Campbell, O. Torres, R. A. Kahn, D. J. Diner, M. C. Helmlinger, D. A. Chu, C. Robles-Gonzalez, and G. De Leeuw (2003a), Coordinated airborne, spaceborne, and ground-based measurements of massive, thick aerosol layers during the dry season in Southern Africa, *J. Geophys. Res*., *108* (D13), 8496, doi:10.1029/2002JD002297.

Schmid, B., D. A. Hegg, J. Wang, D. Bates, J. Redemann, P. B. Russell, J. M. Livingston, H. H. Jonsson, E. J. Welton, J. H. Seinfeld, R. C. Flagan, D. S. Covert, O. Dubovik, A. Jefferson (2003b), Column closure studies of lower tropospheric aerosol and water vapor during ACE-Asia using airborne sunphotometer, airborne in-situ and ship-based lidar measurements, *J. Geophys. Res.* , 108(D23), 8656, doi:10.10292002JD003361.

Schmid B., R. Ferrare, C. Flynn, R. Elleman, D. Covert, A. Strawa, E. Welton, D. Turner, H. Jonsson, J. Redemann, J. Eilers, K. Ricci, A. G. Hallar, M. Clayton, J. Michalsky, A. Smirnov, B. Holben, and J. Barnard (2006), How well do state-of-the-art techniques measuring the vertical profile of tropospheric aerosol extinction compare? *J. Geophys. Res.,111,* 111, D05S07, doi:10.1029/2005JD005837.

Seemann, S. W., J. Li, W. P. Menzel, and L. E. Gumley (2003), Operational retrieval of atmospheric temperature, moisture, and ozone from MODIS infrared radiances, *J. Appl. Meteor*., 42, 1072-1091.

Singh, H. B., et al. (2006), *J. Geophys. Res*., INTEX-A special section, submitted 2006.

Susskind, J., C. Barnet, and J. M. Blaisdell (2003), Retrieval of atmospheric and surface parameters from AIRS/AMSU/HSB data in the presence of clouds, *IEEE Trans. Geosci. Remote Sens*., 41, 390-409.

Susskind, J., C. Barnet, J. Blaisdell, L. Iredell, F. Keita, L. Kouvaris, G. Molnar, and M. Chahine (2006), Accuracy of geophysical parameters derived from Atmospheric Infrared Sounder/Advanced Microwave Sounding Unit as a function of fractional cloud cover, *J. Geophys. Res.*, *111*, D09S17, doi:10.1029/2005JD006272.

Thompson, A. M., J. B. Stone, J. C. Witte, T. L. Kucsera, R. B. Pierce, R. B. Chatfield, O. R. Cooper, B. F. Taubman, S. J. Oltmans, B. J. Johnson, E. Joseph, J. T. Merill, G. Morris, M. J.

Newchurch, F. J. Schmidlin, D. J. Tarasick, and V. Thouret (2005), IONS-2004 (INTEX Ozonesonde Network Study) ozone budgets: Experimental determination and comparison with climatology, *EOS Trans. AGU 86*(52), Fall Meet. Suppl., Abstract A11B-0881.

Tobin, D. C., H. E. Revercomb, R. O. Knuteson, B. M. Lesht, L. L. Strow, S. E. Hannon, W. F. Feltz, L. A. Moy, E. J. Fetzer, and T. S. Cress (2006), Atmospheric Radiation Measurement site atmospheric state best estimates for Atmospheric Sounder temperature and water vapor retrieval validation, *J. Geophys. Res.*, *111*, D09S14, doi:10.1029/2005JD006103.

Whiteman, D. N., F. Russo, B. Demoz, L. M. Miloshevich, I. Veselovskii, S. Hannon, Z. Wang, H. Vömel, F. Schmidlin, B. Lesht, P. J. Moore, A. S. Beebe, A. Gambacorta, and C. Barnet (2006), Analysis of Raman lidar and radiosonde measurements from the AWEX-G field campaign and its relation to Aqua validation, *J. Geophys. Res.*, *111*, D09S09, doi:10.1029/2005JD006429.

J. M. Livingston, SRI International, 333 Ravenswood Avenue, Menlo Park, CA 94025, USA. (john.livingston@sri.com)

S. A. Ramirez, J. Redemann, B. Schmid, S. Howard, J. Pommier, Bay Area Environmental Research Institute, 560 3rd Street West, Sonoma, CA 95476, USA. (s.a.ramirez@mail.arc.nasa.gov, jredemann@mail.arc.nasa.gov, bschmid@mail.arc.nasa.gov , howard@solat.arc.nasa.gov, jpommier@mail.arc.nasa.gov)

P. B. Russell, J. Eilers, W. Gore, NASA Ames Research Center, MS 245-5, Moffett Field, CA 94035-1000, USA. (Philip.B.Russell@nasa.gov, Warren.J.Gore@nasa.gov, jeilers@mail.arc.nasa.gov)

E. J. Fetzer, Jet Propulsion Laboratory, California Institute of Technology, Pasadena, CA 91109, USA. (Eric.J.Fetzer@jpl.nasa.gov)

S. W. Seemann, E. Borbas, University of Wisconsin – Madison, CIMSS, 1225 West Dayton Street, Madison, WI 53706, USA. (swetzel@ssec.wisc.edu, evab@ssec.wisc.edu)

D. Wolfe, NOAA Earth System Research Laboratory, 325 Broadway, Boulder, CO 80305, USA. (Daniel.Wolfe@noaa.gov)

Table 1. Coefficients of *Ingold et al.* [2000] 3-parameter functional fit (2-parameter at altitudes below 4 km) to LBLRTM_v9.2 calculations of water vapor transmittance as a function of slant path water vapor for the AATS-14 940.6-nm channel.

Altitude [km]	a	b	c
0	0.00525	0.6439	1.00000
1	0.00545	0.6331	1.00000
2	0.00557	0.6238	1.00000
3	0.00550	0.6186	1.00000
4	0.00585	0.6052	1.00540
5	0.00617	0.5929	1.00926
6	0.00622	0.5859	1.01006
7	0.00583	0.5892	1.00856
8	0.00506	0.6059	1.00614

Table 2. Comparison of Layer Water Vapor (LWV) retrievals by AATS-14, J31 Vaisala, and AIRS.

		max dist				regression line		rms difference		bias difference	
x	y	[km]	*Qual_Temp_Bot*[1]	n	r^2	slope	intercept	[g/cm^2]	%	[g/cm^2][2]	%[3]
J31 Vaisala	AATS-14			14	0.987	1.000	-0.098	0.127	5.5%	-0.099	4.3%
AATS-14	AIRS	150	2	305	0.542	0.826	0.563	0.513	23.7%	0.183	8.4%
			0	88	0.618	0.830	0.548	0.456	21.5%	0.187	8.8%
		80	2	91	0.763	0.889	0.388	0.341	15.8%	0.148	6.9%
			0	36	0.747	0.814	0.499	0.336	16.4%	0.119	5.8%
J31 Vaisala	AIRS	150	2	305	0.564	0.835	0.454	0.474	20.9%	0.080	3.6%
			0	88	0.639	0.854	0.413	0.411	18.5%	0.089	4.0%
		80	2	91	0.805	0.899	0.278	0.283	12.5%	0.049	2.2%
			0	36	0.807	0.840	0.364	0.275	12.8%	0.021	1.0%

[1] *Qual_Temp_Bot* (= *Qual_Temp_Profile_Bot*) = 0 for highest information content water vapor retrieval [*Fetzer et al.*, 2006]

[2] Calculated as mean(y-x)

[3] Calculated as mean(y-x)/mean(x)

Figure Captions

Figure 1. LBLRTM calculations of water vapor transmittance T_w as a function of slant path water vapor and aircraft altitude for the AATS-14 941-nm channel.

Figure 2. Vertical profiles of CWV calculated from measurements by AATS-14 and the J31 Vaisala HMP243 during INTEX-A/ITCT 2004. Vaisala values have been set equal to the AATS CWV at the top of each profile.

Figure 3. J31 Vaisala minus AATS-14 CWV differences for the vertical profiles shown in Figure 2.

Figure 4. Vertical profiles of water vapor density, ρ_w, for the profiles shown in Figure 2.

Figure 5. For the profiles shown in Figures 2-4, scatterplots of AATS-14 and J31 Vaisala (a) LWV and (b) ρ_w for all profile altitudes.

Figure 6. Comparison of LWV measured by AATS-14 and J31 Vaisala with Ron Brown radiossonde LWV for (a,c) all soundings within 3 hr of a J31 profile, and (b,d) only soundings within 1 hr and 130 km of a J31 profile.

Figure 7. Top: map showing J31 flight track (black thin dashed line) overlain on MODIS grid cells of color-coded MODIS IR TPW for Aqua overpass at 18.1 UT on 21 July 2004. The J31 flight track for the low altitude transect during the period 17.9-18.4 UT has been color-coded by AATS-14 CWV. Bottom: AATS-14 CWV and J31 altitude for the time period 17.6-18.4 UT.

Figure 8. (a) Scatterplot of MODIS TPW and CWV versus AATS CWV. Bars show representative uncertainties. (b) MODIS TPW minus AATS CWV and MODIS CWV minus AATS CWV.

Figure 9. Comparison of MODIS IR and AATS CWV (a) retrievals and (b) differences for 203 MODIS grid cells during 5 MODIS-Aqua (solid circles) and 5 MODIS-Terra (solid triangles) overpasses.

Figure 10. Same as Figure 9, but (a,b) for MODIS-Aqua comparisons only, and (c,d) for MODIS-Terra comparisons only.

Figure 11. (a) Map view of J31 flight track (color coded by aircraft altitude) on 21 July and the center point locations of the 20 AIRS water vapor vertical profile retrievals within 150 km of the J31 17.6-17.9 UT descent (numbers in red give across-track and along-track data indices); (b) Profiles of AIRS CWV retrievals at each of the AIRS locations and AATS-14 and J31 Vaisala CWV measured during the J31 descent.

Figure 12. Profiles of AIRS, AATS-14, and J31 Vaisala LWV_A retrievals within the AIRS retrieval pressure layers for the J31 1739-1756 UT descent and the AIRS profiles shown in Figure 11. Text in each frame gives the mean distance from the J31 profile to the AIRS retrieval center point, in addition to the cross-track and along-track indices of the AIRS location.

Figure 13. Dependence of AIRS minus AATS (a) absolute and (b) relative LWV differences on the distance from the AIRS retrieval location to the mean location of the appropriate J31 profile for 14 separate J31 profiles during 8 Aqua overpasses. Legend gives date, Aqua overpass time, J31 profile times, and vertical extent of each J31 profile.

Figure 14. Comparison of AATS and J31 Vaisala LWV measurements for 14 J31 profiles within 90 minutes of Aqua overflights for which AIRS retrievals of water vapor profiles are available.

Figure 15. Scatterplot comparisons of AIRS and AATS LWV for (a) AIRS retrievals within 150 km of a J31 profile for AIRS retrieval control flag *Qual_Temp_Profile_Bot* = 2, (b) AIRS retrievals within 150 km of a J31 profile for *Qual_Temp_Profile_Bot* = 0, (c) AIRS retrievals within 80 km of a J31 profile for flag *Qual_Temp_Profile_Bot* = 2, (d) AIRS retrievals within 80 km of a J31 profile for *Qual_Temp_Profile_Bot* = 0.

Figure 16. Scatterplot comparisons of AIRS and J31 Vaisala LWV for (a) AIRS retrievals within 150 km of a J31 profile for AIRS retrieval control flag *Qual_Temp_Profile_Bot* = 2, (b) AIRS retrievals within 150 km of a J31 profile for *Qual_Temp_Profile_Bot* = 0, (c) AIRS retrievals within 80 km of a J31 profile for flag *Qual_Temp_Profile_Bot* = 2, (d) AIRS retrievals within 80 km of a J31 profile for *Qual_Temp_Profile_Bot* = 0.

Figure 17. Variation of r^2 for AIRS-AATS and AIRS-Vaisala LWV retrievals as a function of the maximum allowable distance from the J31 profile to the AIRS retrieval location for: (a) *Qual_Temp_Profile_Bot* = 2, and (b) *Qual_Temp_Profile_Bot* = 0. The numbers of AIRS retrievals included in the analyses are also shown.

Figure 18. Results of AIRS and J31 sensor comparisons of LWV_A for AIRS retrievals with *Qual_Temp_Profile_Bot* = 2 and within 150 km of a J31 vertical profile. (a) Means (open circles with solid lines) and ranges (dashed lines) of AIRS and AATS LWV_A profile retrievals, numbers of AIRS and AATS retrievals at each altitude; (b) absolute AIRS minus AATS LWV_A biases and

rms differences; (c) relative AIRS minus AATS LWV_A biases and rms differences; (d-f) same as (a-c) but for AIRS-J31 Vaisala comparisons.

Figure 19. Same as Figure 18, but for AIRS retrievals with *Qual_Temp_Profile_Bot* = 0 and within 150 km of a J31 vertical profile.

Figure 20. Same as Figure 18, but for AIRS retrievals with *Qual_Temp_Profile_Bot* = 2 and within 80 km of a J31 vertical profile.

Figure 21. Same as Figure 19, but for AIRS retrievals with *Qual_Temp_Profile_Bot* = 0 and within 80 km of a J31 vertical profile.